INTERNATIONAL JOURNAL OF CONTROL
2019, VOL. 92, NO. 1, 77–99
https://doi.org/10.1080/00207179.2017.1308556

Taylor & Francis
Taylor & Francis Group

Parabolic PDE-based multi-agent formation control on a cylindrical surface

Jie Qi[a,b], Shu-Xia Tang[c] and Chuan Wang[a,b]

[a]School of Information Science and Technology, Donghua University, Shanghai, China; [b]Engineering Research Center of Digitized Textile and Fashion Technology, Ministry of Education, Donghua University, Shanghai, China; [c]Department of Mechanical & Aerospace Engineering, University of California, San Diego, CA, USA

ABSTRACT

This paper considers the modelling and control design of the multi-agent systems in the 3-D space. The communication graph of the agents is a mesh-grid 2-D cylindrical surface. Different from most existing literatures, where the agents are modelled by ordinary differential equations (ODEs), we treat the agents as a continuum in this paper. More specifically, we model the collective dynamics of the agents by two reaction–advection–diffusion 2-D partial differential equations (PDEs). The PDE states represent the agent positions, and the equilibria correspond to possible formation manifolds. These PDEs can be open-loop unstable, and the boundary stabilisation problem of the PDEs on the cylindrical surface is solved using the backstepping method. An all-explicit observer-based output control scheme is constructed, which is distributed in the sense that each agent only needs local information. Closed-loop exponential stability in the L^2, H^1, and H^2 spaces is proved for the controller designs. Numerical simulations illustrate the effectiveness of our proposed approach.

ARTICLE HISTORY
Received 31 January 2016
Accepted 15 March 2017

KEYWORDS
Backstepping; multi-agent formation control; parabolic PDEs; boundary control; cylindrical surface

1. Introduction

Multi-agent formation control has attracted considerable attention in recent years due to its wide potential applications, such as surveillance and reconnaissance (Kopfstedt, Mukai, Fujita, & Ament, 2008), search and rescue (Shiroma, Chiu, Sato, & Matsuno, 2005), large area exploration (Zhang & Leonard, 2010), contour or structure mapping (Han, Xu, Di, & Chen, 2013; Tavakoli, Cabrita, Faria, Marques, & de Almeida, 2012), science imaging (Dunbabin & Marques, 2012), sampling the ocean surface (Kalantar & Zimmer, 2007) and space missions (Krieger, Hajnsek, Papathanassiou, Younis, & Moreira, 2010). Cooperative formation control aims to drive a collection of autonomous agents to reach prescribed target orbits in a distributed way based on local information, instead of the global information (Oh, Park, & Ahn, 2015).

There are a vast collection of existing works on multi-agent formation control which are based on traditional discrete ordinary differential equation (ODE) models (see, Bullo & Martinez, 2009; Cao, Yu, Ren, & Chen, 2013; Hatanaka, Chopra, Fujita, & Spong, 2015; Olfati-Saber, Fax, & Murray, 2007; Ren, Beard, & Atkins, 2005). The consensus control algorithm plays a crucial role. Actually, many formation controllers can be treated as special cases of consensus-based controllers, whose stabilities are analysed under the framework of graph Laplace matrices. Ren and Sorensen (2008) design a leader–follower distributed formation control and present a state estimation architecture. Dasdemir and Loría (2014) introduce a uniform global exponential stable consensus formation control law in a spanning-tree topology for the situation that the position measurements may be lost over the communication interruption intervals. Another approach, hinging on the use of potential functions, can be found in Krick, Broucke, and Francis (2009), which designs a gradient control law for the agents to form the desired formation based on a potential function of the distances among the neighbourhood agents. The traditional ODE methods have the disadvantage that the number of ODEs increases as the agent population grows. In practice, it would be impossible to control a multi-agent system with a huge number of nodes.

For large-scale multi-agent systems, a new continuum-based viewpoint has arisen, leaning heavily on partial differential equation (PDE) models (see Blondel, Hendrickx, & Tsitsiklis, 2010; Canuto, Fagnani, & Tilli, 2008; Helbing, 2001; Sarlette & Sepulchre, 2009). Ferrari-Trecate, Buffa, and Gati (2006) propose a framework of partial difference equations (PDEs) over graphs to analyse the collective dynamics of the multi-agent systems, which in turn provides the fundamental basis to employ PDEs to model multi-agent systems. Since the (graph) Laplace control law for the state consensus (Olfati-Saber &

CONTACT Shu-Xia Tang s74tang@uwaterloo.ca

Murray, 2004) can be formulated as a linear PDE which behaves like a heat equation over the graph, the Laplace operator in a PDE could play the role of consensus control. The selected discretisation schemes for a PDE with respect to the spatial coordinates determine the underlying communication topology connecting different agents. In particular, the application of finite-difference approximations results in the space variable(s) being mapped as the agent index(es), and the spatial derivatives being transformed into links between neighbours (see Barooah, Mehta, & Hespanha, 2009; Qi, Vázquez, & Krstic, 2015), which allow the collective dynamics of a large group of discrete agents to be formulated as a PDE. Hao and Barooah (2012) also analyse the approximation error between the PDE and the corresponding discretised agent system, which states PDE is an accurate approximation of the coupled-ODE model. Kim, Kim, Natarajan, Kelly, and Bentsman (2008) employ an adaptive control law for a multi-agent PDE system to achieve desired formation. Meurer and Krstic (2011) design a feedforward controller for multi-agent finite-time deployment by using a flatness-based motion planning method for PDEs. A 1-D linear reaction–advection–diffusion PDE is used in Frihauf and Krstic (2011) for leader-enabled deployment onto planar curves. Ghods and Krstic (2012) incorporate extremum seeking in a PDE model for multi-agent deployment around a source. Hao, Barooah, and Mehta (2011) introduce a wave-like PDE to study the scaling laws of stability margin for large vehicular formations by means of PDE eigenvalue analysis. Hyperbolic models have also been used to analyse networks of oscillators in Mauroy and Sepulchre (2013). In this paper, we employ two 2-D reaction–advection–diffusion PDEs to model the dynamics of a large-scale multi-agent system, where the PDE states denote the positions of the agents. The first PDE is complex-valued, with the real and imaginary parts denoting the state components under x and y coordinates, respectively. The second PDE is real-valued and describes the state evolution following the z coordinate (height). The advection and diffusion terms help generate all possible equilibria of the PDEs, which could be treated as rich and interesting desired formation profiles. As will be seen later, the transition from one formation to another formation can be achieved by changing the equilibria.

Note that the desired formations can be open-loop unstable, and we use the backstepping method (Krstic & Smyshlyaev, 2008) for designing boundary controllers to stabilise the formations. Backstepping has proved to be good at explicit boundary controller design for 1-D PDE (Smyshlyaev & Krstic, 2004). By only adding control inputs to a few agents, namely the leader agents on the boundary, of the whole multi-agents network through applying the boundary control, we achieve the formation control goal. This is consistent with the conception of pinning control strategy (Wang & Su, 2014) in that the leader agents are the selected pinning agents to be controlled. More importantly, it greatly reduces the cost of calculation with the system modelled by ODEs. Furthermore, there are only a few literatures on backstepping control of higher dimensional PDEs. Vázquez and Krstic (2007) use Fourier transformation to first reduce the dimension and then design boundary controllers for the resulting 1-D PDEs, while Vázquez, Trélat, and Coron (2008) employ Fourier series expansion to study a periodical boundary problem. For the periodical boundary of the cylindrical topology in the paper, we employ Fourier series to expand the 2-D PDEs. Then, for each Fourier coefficient which satisfies a 1-D PDE, we design the backstepping control laws, where the kernel equations are solved to its explicit form. Finally, we assemble all the Fourier coefficients to get the boundary control for the 2-D PDEs. In order to reduce the cost of information exchange between the leader agents and follower agents, we design an observer also in explicit form to estimate the positions of all the agents, which are required in the leaders' feedback control law, from only one boundary measurement. By using the observer, the leaders only need to interact with their nearest neighbours for obtaining the positions. Moreover, since only the leaders need to know the desired formation in advance (they are selected pining agents), this would also decrease the cost of the system.

This model could serve as an extension of the one proposed in Qi et al. (2015), where it is defined on a disk, and the model in this paper is defined on a cylindrical surface, parameterised in the cylindrical coordinates (r, θ, s) with a constant radium. The cylindrical surface, as the topology of the continuum agents, could generate the cylindrical and conical surface that cannot be generated by the use of a disk topology (see Qi et al., 2015). Note that cylinders and cones exist broadly in real world, and also that the cylindrical and conical formations are significant for multi-agent system in applications. For example, a group of sensors takes a cylindrical formation around the pipes to detect possible leakage of offshore pipes during gas or crude oil transportation (Xu, Dong, Ren, Jiang, & Yu, 2014).

In addition, we show the closed-loop stability with respect to the L^2, H^1, and H^2 norms, respectively, which guarantees a good system behaviour. In order for 2-D PDEs to have state continuity, H^2 norm stability is needed, which in turn guarantees the connection of the topology. The continuity of the state variables implies that the agents which are neighbours in topology are also close in physical space. Each agent has a limited

communication capability which allows it to interact only with agents nearby. Hence, H^2 norm stability of the closed-loop control system is necessary for the proposed control laws to keep the topology unchanged and connected over time, which avoid extra cost for preserving topology connectivity (see Wang & Su, 2014).

In our simulation, the PDEs are discretised via a three-point central difference scheme to get a control law for each agent, which imposes an initial topology of a meshgrid on cylindrical surface for the agents interacting with each other. Namely, each inner agent has four neighbours, while each agent at the boundary has three neighbours. The topology keeps unchanged over time by applying the proposed method. The designed controllers are actuated by a few leader agents located at the boundary. The numerical simulations are consistent with the theoretical results, which illustrate that the proposed control laws also achieve smooth transitions among different formations. Furthermore, we study the collision among agents by using simulation; in the numerical example of the paper, no collision occurs, given the initial positions of non-collision.

The remaining parts of this paper are organised as follows. Section 2 presents the model and some potential formation profiles for the agents. Section 3 focuses on the design of a boundary control law for the system in a cylindrical surface domain. For the resulting closed-loop system with the boundary control, it is proven in Section 4 that the desired agent formation profiles are exponential stable with respect to the H^2 norm. Then, we introduce a boundary observer and prove the H^2 exponential stability of the output-feedback closed-loop control system in Section 5. By means of the finite difference methods, we relate the PDE control designs with the distributed control laws for the agents in Section 6. Moreover, we give some numerical simulation results to demonstrate the effectiveness of the proposed control laws. We conclude this paper with some remarks in Section 7. Finally, we end this article with two appendices that contain some necessary details.

2. Modelling the multi-agent system

Consider a group of agents labelled by (i, j), $i = 1, \dots, N, j = 1, \dots, M$, which move in the 3-D space under the coordinate axes (x, y, z). To simplify the expression, we use a complex-valued variable $u = x + jy$ to denote the state components on the axes (x, y). In the most straightforward ODE models, the consensus control laws (see Olfati-Saber et al., 2007) for each agent (i, j) are usually formulated as integrators:

$$\frac{du_{i,j}}{dt} = \sum_{(m,l)\in\mathcal{N}_{(i,j)}} \alpha^{(i,j)}_{(m,l)}(u_{m,l} - u_{i,j}), \tag{1}$$

$$\frac{dz_{i,j}}{dt} = \sum_{(m,l)\in\mathcal{N}_{(i,j)}} \beta^{(i,j)}_{(m,l)}(z_{m,l} - z_{i,j}), \tag{2}$$

where $\mathcal{N}_{(i,j)}$ denotes the set of all the other agents that share information with each agent (i, j), called as its neighbours. The constants $\alpha^{(i,j)}_{(m,l)}, \beta^{(i,j)}_{(m,l)}$ represent the corresponding weights of credibility that are put on the information from each neighbour. Consider an indirect topology graph on a cylindrical surface (see Figure 1), which defines the neighbour set of each agent. Our control objective is to drive the system into some desired formation profiles on this surface.

When the number of the agents is large, more specifically, if M and N are large, then we can treat the whole of the agents as a continuum. This allows to map the discrete identification (ID) numbers (i, j) of the agents (θ_i, s_j) into the coordinates on the cylindrical surface $\Omega = \{(\theta, s) : -\pi \le \theta < \pi, 0 \le s \le 1\}$, that is, $(\theta_i, s_j) \to (\theta, s)$ as $M, N \to \infty$. Correspondingly, the (large scale) multi-agent systems can be modelled as PDEs. In this section, we would like to employ (linear parabolic) PDEs instead, for modelling the collective dynamics of the multi-agent systems. The equilibria of the PDEs, which fully depend on the chosen models, stand for the corresponding desired formation profiles.

Ferrari-Trecate et al. (2006) state that the Laplace operator in the PDE plays the role of the consensus law proposed in Olfati-Saber and Murray (2004). Indeed, all the (partial) derivatives of the state with respect to the state variable can stand for some communication graphs among the agents. Thus, the collective dynamics of the agent system can be modelled by a system of two reaction–advection–diffusion PDEs as follows:

$$u_t(t, \theta, s) = \Delta u(t, \theta, s) + \beta_1 u_s(t, \theta, s) + \lambda_1 u(t, \theta, s), \tag{3}$$

$$z_t(t, \theta, s) = \Delta z(t, \theta, s) + \beta_2 z_s(t, \theta, s) + \lambda_2 z(t, \theta, s), \tag{4}$$

for $(t, \theta, s) \in \mathbb{R}^+ \times \Omega$, $u, \lambda_1, \beta_1 \in \mathbb{C}$, $z, \lambda_2, \beta_2 \in \mathbb{R}$. Δ denotes the Laplace operator, that is,

$$\Delta u(t, \theta, s) = u_{\theta\theta}(t, \theta, s) + u_{ss}(t, \theta, s), \tag{5}$$

$$\Delta z(t, \theta, s) = z_{\theta\theta}(t, \theta, s) + z_{ss}(t, \theta, s). \tag{6}$$

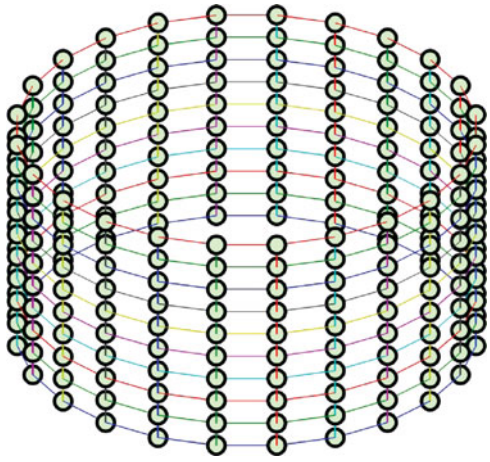

Figure 1. Cylindrical surface topology defining the communication relationship among agents. The agents at the uppermost and lowermost layers are leaders. Each follower has four neighbours.

(θ, s) are the spatial variables, which also serve as the IDs of the agents on the communication topology. The boundary conditions are

$$u(t,\theta,0) = f_1(\theta), \quad u(t,\theta,1) = g_1(\theta) + U(t,\theta), \tag{7}$$

$$u(t,-\pi,s) = u(t,\pi,s), \tag{8}$$

$$z(t,\theta,0) = f_2(\theta), \quad z(t,\theta,1) = g_2(\theta) + Z(t,\theta), \tag{9}$$

$$z(t,-\pi,s) = z(t,\pi,s), \tag{10}$$

where $f_1(\theta)$, $g_1(\theta)$ and $f_2(\theta)$, $g_2(\theta)$ are non-zero and bounded boundary conditions for the states u and z, respectively, which represent (open-loop) formation of the leaders. $U(t, \theta)$ and $Z(t, \theta)$ are the to-be-designed boundary controllers at the horizontal and vertical coordinates, respectively, to stabilise the system to some equilibria. Moreover, (8) and (10) are periodic boundary conditions for the cylinder surface. Following the conception of boundary actuation, the agents at the boundary are selected as leaders, which are located at the uppermost and lowermost layers in the topology surface (see Figure 1).

The steady-state solutions $(\bar{u}(\theta, s), \bar{z}(\theta, s))$ to (3)–(10) satisfy the following PDEs:

$$\Delta\bar{u}(\theta,s) + \beta_1\bar{u}_s(\theta,s) + \lambda_1\bar{u}(\theta,s) = 0, \tag{11}$$

$$\Delta\bar{z}(\theta,s) + \beta_2\bar{z}_s(\theta,s) + \lambda_2\bar{z}(\theta,s) = 0, \tag{12}$$

with

$$\bar{u}(\theta,0) = f_1(\theta), \quad \bar{u}(\theta,1) = g_1(\theta), \tag{13}$$

$$\bar{u}(0,s) = \bar{u}(2\pi,s), \tag{14}$$

$$\bar{z}(\theta,0) = f_2(\theta), \quad \bar{z}(\theta,1) = g_2(\theta), \tag{15}$$

$$\bar{z}(0,s) = \bar{z}(2\pi,s). \tag{16}$$

The explicit solution for the complex-valued state is given by

- If $a := \beta_1^2 - 4\lambda_1 + 4n^2 > 0$, then

$$\bar{u}(\theta,s) = \sum_{n=-\infty}^{\infty} \mathrm{e}^{\mathrm{j}n\theta - 1/2\beta_1 s}\left(A_n\mathrm{e}^{\sqrt{a}s} + B_n\mathrm{e}^{-\sqrt{a}s}\right), \tag{17}$$

- If $a = 0$, then

$$\bar{u}(\theta,s) = \sum_{n=-\infty}^{\infty} \mathrm{e}^{\mathrm{j}n\theta}\left(A_n\mathrm{e}^{-\frac{1}{2}\beta_1 s} + B_n s\mathrm{e}^{-\frac{1}{2}\beta_1 s}\right), \tag{18}$$

- If $a < 0$, then

$$\bar{u}(\theta,s) = \sum_{n=-\infty}^{\infty} \mathrm{e}^{\mathrm{j}n\theta - 1/2\beta_1 s}\left(A_n\cos\left(\frac{1}{2}\sqrt{-a}s\right) + B_n\sin\left(\frac{1}{2}\sqrt{-a}s\right)\right), \tag{19}$$

where A_n's and B_n's are all constants depending on the boundary condition (13), (14). The equilibria $\bar{z}$ can be obtained in a similar way. These equilibria $(\bar{u}, \bar{z})$ can serve as the desired positions for all the agents to reach, then Equations (11)–(16) characterise all achievable 3-D deployments. Once the agents arrive at these steady-state positions, they would stay there forever, unless there are some external forces that make them leave. Figure 2 shows four possible formation manifolds upon different boundaries and parameters.

Note that for large values of $\mathrm{Re}(\lambda_1)$ and λ_2, systems (3)–(10) could be open-loop unstable. In this case, the agents would not move spontaneously (without a control) to the desired position (formation profiles) from any initial positions except the equilibria. Then, it is necessary to design stabilising (boundary) controllers, which are the feedback control laws actuated by the leaders.

Let

$$\tilde{u}(t,\theta,s) = u(t,\theta,s) - \bar{u}(\theta,s), \tag{20}$$

$$\tilde{z}(t,\theta,s) = z(t,\theta,s) - \bar{z}(\theta,s), \tag{21}$$

then, we arrive at the following (error) system of equations:

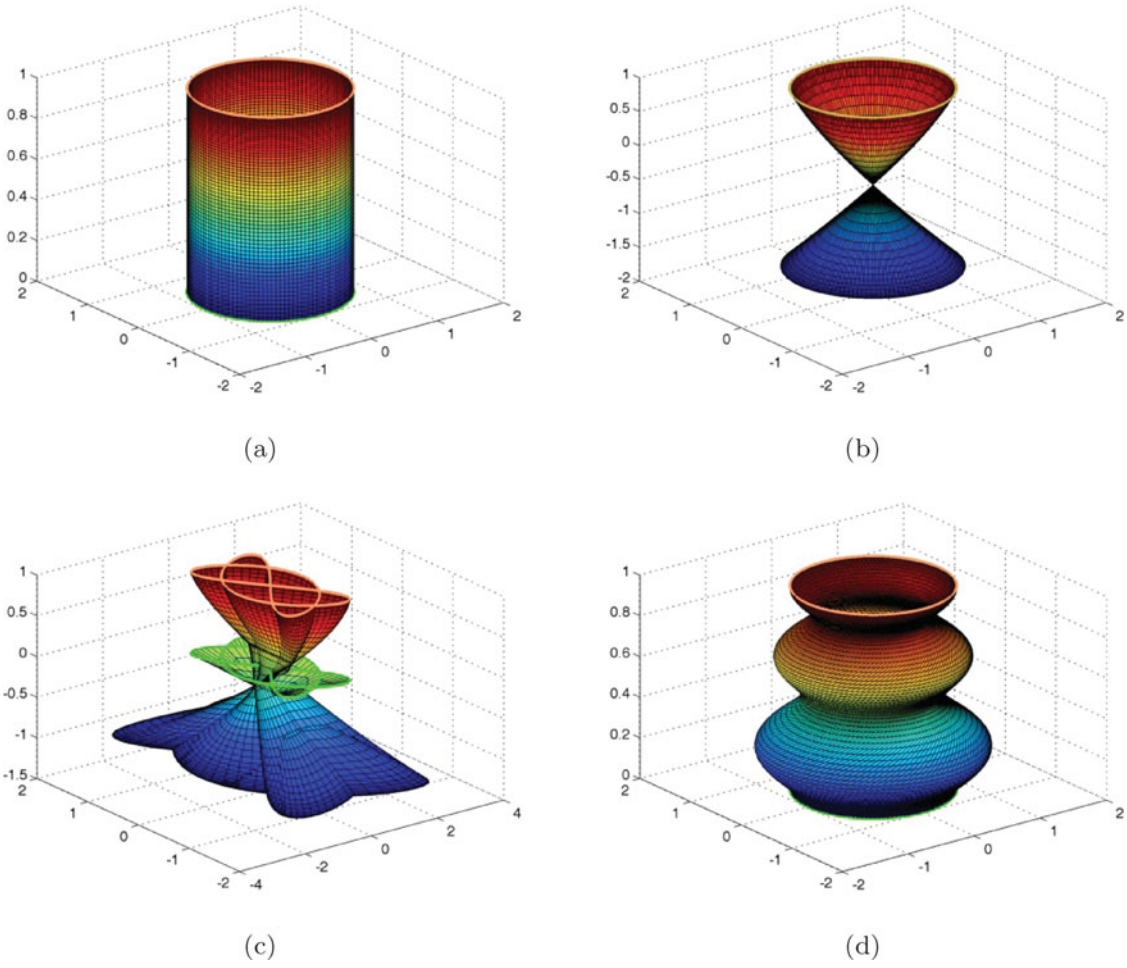

Figure 2. Agent formation manifolds. The green and orange curves represent the formation shapes on the boundaries $s = 0$ and $s = 1$, which denote the corresponding positions of the leaders. (a) The boundaries are $f_1(\theta) = g_1(\theta) = e^{j\theta}$ and $f_2(\theta) = 0$, $g_2(\theta) = 1$ with the parameters $\lambda_1 = 1$, $\lambda_2 = 1$ and $\beta_1 = \beta_2 = 0$. (b) The boundaries are $f_1(\theta) = g_2(\theta) = e^{j\theta}$ and $f_2(\theta) = 1$, $g_2(\theta) = 1$ with the parameters $\lambda_1 = 30$, $\lambda_2 = 20$ and $\beta_1 = \beta_2 = 0$. (c) The boundaries are $f_1(\theta) = g_1(\theta) = \frac{1}{2}e^{-j3\theta} - \frac{1}{2}e^{-j2\theta} + \frac{1}{2}e^{j2\theta} + \frac{1}{2}e^{j3\theta}$ and $f_2(\theta) = 0$, $g_2(\theta) = 1$, with the parameters $\lambda_1 = 30$, $\lambda_2 = 18$, $\beta_1 = 2$ and $\beta_2 = 0$. (d) The boundaries are $f_1(\theta) = g_1(\theta) = e^{j\theta}$ and $f_2(\theta) = 0$, $g_2(\theta) = 1$, with the parameters $\lambda_1 = 60$, $\lambda_2 = 1$, $\beta_1 = 1 + 3j$ and $\beta_2 = 0$

$$\tilde{u}_t(t,\theta,s) = \Delta\tilde{u}(t,\theta,s) + \lambda_1\tilde{u}(t,\theta,s) + \beta_1\tilde{u}_s(t,\theta,s), \tag{22}$$

$$\tilde{z}_t(t,\theta,s) = \Delta\tilde{z}(t,\theta,s) + \lambda_2\tilde{z}(t,\theta,s) + \beta_2\tilde{z}_s(t,\theta,s), \tag{23}$$

with the boundary conditions

$$\tilde{u}(t,\theta,0) = 0, \quad \tilde{u}(t,\theta,1) = \tilde{U}(t,\theta), \tag{24}$$

$$\tilde{u}(t,0,s) = \tilde{u}(t,2\pi,s), \tag{25}$$

$$\tilde{z}(t,\theta,0) = 0, \quad \tilde{z}(t,\theta,1) = \tilde{Z}(t,\theta), \tag{26}$$

$$\tilde{z}(t,0,s) = \tilde{z}(t,2\pi,s), \tag{27}$$

where

$$\tilde{U}(t,\theta) = U(t,\theta). \tag{28}$$

Since the $\tilde{u}$ and $\tilde{z}$ systems are uncoupled, they can be analysed separately. We shall only analyse the dynamics of $\tilde{u}$ in detail, and the results for $\tilde{z}$ can be derived in a similar form. In the next sections, we focus on stabilising control designs for the $\tilde{u}$-system (22), (24) and (25).

3. Backstepping boundary control

We first transform the system (22), (24) and (25) into a simpler form (without the advection term) through the following map:

$$v(t,\theta,s) = e^{\frac{1}{2}\beta_1 s}\tilde{u}(t,\theta,s), \tag{29}$$

In Appendix 1, we give more discussion about the transformation (29).

Then, the system becomes

$$v_t(t,\theta,s) = \Delta v(t,\theta,s) + \lambda v(t,\theta,s), \tag{30}$$

$$v(t,\theta,0) = 0, \quad v(t,\theta,1) = V(t,\theta), \tag{31}$$

$$v(t,0,s) = v(t,2\pi,s), \tag{32}$$

where

$$\lambda = \lambda_1 - \frac{1}{4}\beta_1^2, \tag{33}$$

$$V(t,\theta) = e^{\frac{1}{2}\beta_1}\tilde{U}(t,\theta) = e^{\frac{1}{2}\beta_1}U(t,\theta). \tag{34}$$

It is obvious that the system (22), (24) and (25) and the system (30)–(32) are equivalent. Thus, we would like to stabilise the system (30)–(32) to the origin. In what follows, we shall design a feedback control law by using a backstepping-based method.

3.1 PDE control design for the fourier series coefficients

By using the Fourier series expansion, we first derive the PDE systems in which the system states are the corresponding Fourier coefficients. The Fourier coefficients are independent of the angular argument, and as a result, the system dimension is reduced to one. We design the boundary controller for each of the resultant PDE system by backstepping method. Then, we obtain the controller for the two-dimensional PDE by inverting the Fourier transformation, i.e. summing the boundary controllers multiplied by $e^{j\theta}$. We expand the system state of (30) and the boundary control in (32) as Fourier series:

$$v(t,\theta,s) = \sum_{n=-\infty}^{\infty} v_n(t,s)\mathrm{e}^{\mathrm{j}n\theta}, \tag{35}$$

$$V(t,\theta) = \sum_{n=-\infty}^{\infty} V_n(t)\mathrm{e}^{\mathrm{j}n\theta}, \tag{36}$$

where the coefficients v_n and V_n, for $n \in \mathbb{Z}$, satisfy

$$v_n(t,s) = \frac{1}{2\pi}\int_{-\pi}^{\pi} v(t,s,\psi)\mathrm{e}^{-\mathrm{j}n\psi}d\psi, \tag{37}$$

$$V_n(t) = \frac{1}{2\pi}\int_{-\pi}^{\pi} V(t,\psi)\mathrm{e}^{-\mathrm{j}n\psi}d\psi. \tag{38}$$

Each coefficient $v_n(t,r), n \in \mathbb{Z}$ verifies the following PDE:

$$v_{nt}(t,s) = v_{nss}(t,s) - n^2 v_n(t,s) + \lambda v_n(t,s), \tag{39}$$

evolving in $(t,s) \in \mathbb{R}^+ \times [0,1]$, with the boundary condition

$$v_n(t,0) = 0, v_n(t,1) = V_n(t). \tag{40}$$

Since these PDEs are uncoupled, we can independently design a feedback controller V_n to stabilise each v_n system. After that, we can use (36) to find U, by assembling all the designed V_n's.

Following the PDE backstepping method proposed in Krstic and Smyshlyaev (2008), our approach for designing the controller $V_n(t)$ is to seek a transformation to map the system (39), (40) into the following exponential stable target system:

$$w_{nt}(t,s) = w_{nss}(t,s) - n^2 w_n(t,s) \tag{41}$$

with the following boundary condition:

$$w_n(t,0) = 0, w_n(t,1) = 0. \tag{42}$$

Postulate the transformation as follows:

$$w_n(t,s) = v_n(t,s) - \int_0^s K_n(s,\tau)v_n(t,\tau)d\tau, \tag{43}$$

where the to-be-determined kernel $K_n(s,\tau)$ is defined on $\mathcal{T}_s = \{(s,\tau) : 0 \le \tau \le s \le 1\}$. By substituting the transformation (43) into the target system (41), (42), performing differentiation and integration by parts (see Smyshlyaev & Krstic, 2004), we arrive at the following hyperbolic PDE for the transformation kernel:

$$K_{nss}(s,\tau) - K_{n\tau\tau}(s,\tau) = \lambda K_n(s,\tau) \tag{44}$$

with the boundary condition

$$K_n(s,0) = 0, \quad K_n(s,s) = -\frac{\lambda}{2}s. \tag{45}$$

From the result for the solution to (4.15) in Krstic and Smyshlyaev (2008), we have the following explicit expression for the kernel:

$$K_n(s,\tau) = -\lambda\tau\frac{\mathrm{I}_1\left[\sqrt{\lambda(s^2-\tau^2)}\right]}{\sqrt{\lambda(s^2-\tau^2)}}, \tag{46}$$

where I_1 is the first-order modified Bessel function of the first-kind. Note that all the kernels $K_n(s,\tau)$ are independent of n, and, thus, we write

$$K_n(s,\tau) \triangleq K(s,\tau) \in \mathcal{C}^\infty(\mathcal{T}). \tag{47}$$

By setting $s=1$ in (43) and applying the boundary conditions (40), (42), we immediately obtain the following control law $V_n(t)$ as a feedback of all the values $\upsilon_n(t,\tau)$ for $\tau \in (0,1)$:

$$\begin{aligned} V_n(t) &= \int_0^1 K_n(1,\tau)\upsilon_n(t,\tau)d\tau \\ &= -\int_0^1 \lambda\tau \frac{\mathrm{I}_1\left[\sqrt{\lambda(1-\tau^2)}\right]}{\sqrt{\lambda(1-\tau^2)}}\upsilon_n(t,\tau)d\tau. \end{aligned} \tag{48}$$

3.2 PDE controller for the original (error) system

Let

$$w(t,\theta,s) = \sum_{n=-\infty}^{\infty} w_n(t,s)\mathrm{e}^{\mathrm{j}n\theta}, \tag{49}$$

then, from the transformations (35) and (43), we have the following relation between $w(t,\theta,s)$ and $\upsilon(t,\theta,s)$:

$$\begin{aligned} w(t,\theta,s) &= \sum_{n=-\infty}^{\infty} \upsilon_n(t,s)\mathrm{e}^{\mathrm{j}n\theta} \\ &\quad - \sum_{n=-\infty}^{\infty} \int_0^s K(s,\tau)\upsilon_n(t,\tau)\mathrm{e}^{\mathrm{j}n\theta}d\tau \\ &= \upsilon(t,\theta,s) - \int_0^s K(s,\tau)\upsilon(t,\theta,\tau)d\tau. \end{aligned} \tag{50}$$

Moreover, we have the following (exponentially stable) system for w:

$$w_t(t,\theta,s) = \Delta w(t,\theta,s), \tag{51}$$

$$w(t,\theta,0) = 0, \quad w(t,\theta,1) = 0. \tag{52}$$

From (36) and (48), we get the following control law $V(t,\theta)$:

$$V(t,\theta) = -\int_0^1 \lambda\tau \frac{\mathrm{I}_1\left[\sqrt{\lambda(1-\tau^2)}\right]}{\sqrt{\lambda(1-\tau^2)}}\upsilon(t,\theta,\tau)d\tau, \tag{53}$$

which is a feedback of all the state values $\upsilon(t,\theta,\tau)$ for $\tau \in (0,1)$. In Appendix 2, we design the controllers for the two coupled real-valued PDEs corresponding to the real and imaginary parts of υ, respectively, which is shown to be equivalent to (53).

Back to the original u-system (3), (7), (8), we get the following boundary controller:

$$\begin{aligned} U(t,\theta) &= e^{-\frac{1}{2}\beta_1}V(t,\theta) \\ &= -\int_0^1 \lambda\tau \frac{\mathrm{I}_1\left[\sqrt{\lambda(1-\tau^2)}\right]}{\sqrt{\lambda(1-\tau^2)}}\mathrm{e}^{-\frac{1}{2}\beta_1(1-\tau)}(u(t,\theta,\tau) \\ &\quad - \bar{u}(\theta,\tau))d\tau, \end{aligned} \tag{54}$$

where the first line used (20) and (25), the second line used (13), (20), (34) and (53). The control law (54) for the leader agents on the boundary could help achieve the desired stable formation, in which the formation shape $\bar{u}(\theta,s)$ and formation boundary $g_1(\theta)$ can be precomputed.

The real-valued z-model for the height coordinate can be regarded as a special case of the complex-valued u-model (22), (24), (25). Thus, by following a similar procedure, a stabilising control law actuated by the leaders for the z system is obtained as

$$\begin{aligned} Z(t,\theta) &= -\int_0^1 \lambda\tau \frac{\mathrm{I}_1\left[\sqrt{\lambda(1-\tau^2)}\right]}{\sqrt{\lambda(1-\tau^2)}}\mathrm{e}^{-\frac{1}{2}\beta_1(1-\tau)}(z(t,\theta,\tau) \\ &\quad - \bar{z}(\theta,\tau))d\tau. \end{aligned} \tag{55}$$

3.3 Inverse transformation from u to w

The transformation (50) from u to w is invertible and the inverse transformation is

$$\upsilon(t,\theta,s) = w(t,\theta,s) + \int_0^s G(s,\tau)w(t,\theta,\tau)d\tau, \tag{56}$$

where

$$G(s,\tau) = -\lambda\tau \frac{\mathrm{J}_1\left[\sqrt{\lambda(s^2-\tau^2)}\right]}{\sqrt{\lambda(s^2-\tau^2)}} \in \mathcal{C}^\infty(\mathcal{T}). \tag{57}$$

4. Stability analysis

In this section, we investigate the stability of the closed-loop u-system (3), (7), (8) with the controller (54). Given that the considered domain is two-dimensional, a result at least in the Sobolev space H^2 is required (see Brezis, 2010), to have the continuity of the state variables. Our definitions of the partial derivatives under the cylindrical coordinates (r,θ,s) follow from those defined under the Cartesian coordinates (x,y,s). Given a function $\chi(r,\theta,s)$

$\in C^1$, it can be derived from the chain rule that

$$\frac{\partial \chi}{\partial x} = \cos\theta \frac{\partial \chi}{\partial r} - \frac{\sin\theta}{r}\frac{\partial \chi}{\partial \theta}, \tag{58}$$

$$\frac{\partial \chi}{\partial y} = \sin\theta \frac{\partial \chi}{\partial r} + \frac{\cos\theta}{r}\frac{\partial \chi}{\partial \theta}, \quad \frac{\partial \chi}{\partial s} = \frac{\partial \chi}{\partial s}. \tag{59}$$

Let $r = 1$, then (58), (59) become

$$\frac{\partial \chi}{\partial x} = -\sin\theta \frac{\partial \chi}{\partial \theta}, \quad \frac{\partial \chi}{\partial y} = \cos\theta \frac{\partial \chi}{\partial \theta}, \quad \frac{\partial \chi}{\partial s} = \frac{\partial \chi}{\partial s}. \tag{60}$$

Based on (60), we give the following definitions of the L^2, H^1 and H^2 norms.

Definition 4.1: The L^2 norm on the cylindrical surface $\|\cdot\|_{L^2}$ is defined as

$$\|\chi(\theta, s)\|_{L^2} = \left(\int_0^1 \int_{-\pi}^{\pi} |\chi(\theta, s)|^2 d\theta ds\right)^{1/2}, \quad \forall \chi(\theta, s) \in L^2((0,1) \times (-\pi, \pi)). \tag{61}$$

The Sobolev norm $\|\cdot\|_{H^1}$ is defined as

$$\|\chi(\theta, s)\|_{H^1}^2 = \|\chi(\theta, s)\|_{L^2}^2 + \|\chi_\theta(\theta, s)\|_{L^2}^2 + \|\chi_s(\theta, s)\|_{L^2}^2, \forall \chi(\theta, s) \in H^1((0,1)(-\pi, \pi)). \tag{62}$$

The Sobolev norm $\|\cdot\|_{H^2}$ is defined as

$$\|\chi(\theta, s)\|_{H^2}^2 = \|\chi\|_{H^1}^2 + \|\chi_{\theta\theta}\|_{L^2}^2 + 2\|\chi_{\theta s}\|_{L^2}^2 + \|\chi_{ss}\|_{L^2}^2 + \|\chi_\theta\|_{L^2}^2, \forall \chi(\theta, s) \in H^2((0,1)(-\pi, \pi)). \tag{63}$$

We know that the u-system and the v-system (30)–(32) are equivalent. Moreover, based on the transformations (50), (56) between the v-system (30)–(32) and the w-system (51)–(52), the following proposition states the equivalence of the L^2, H^1 and H^2 norms of v and those of w, respectively.

Proposition 4.1: *Let $\chi(\theta, s)$ be related to $\Xi(\theta, s)$ by follows:*

$$\chi(\theta, s) = \Xi(\theta, s) + \int_0^s L(s, \tau)\Xi(\theta, \tau)d\tau, \tag{64}$$

where $L(s, \tau) \in \mathcal{C}^2(\mathcal{T})$. Then,

$$\|\chi\|_{L^2} \le C_0 \|\Xi\|_{L^2}, \tag{65}$$

$$\|\chi\|_{H^1} \le C_1 \|\Xi\|_{H^1}, \tag{66}$$

$$\|\chi\|_{H^2} \le C_2 \|\Xi\|_{H^2}, \tag{67}$$

where the constants C_i, $i = 1, 2, 3$ depend only on $L(s, \tau)$.

Proof: Since $L(s, \tau) \in \mathcal{C}^2(\mathcal{T})$, then there exist positive constants M, M_s, M_τ, M_{ss} such that for any $(s, \tau) \in \mathcal{T}$,

$$|L(s, \tau)| \le M, \quad |L_s(s, \tau)| \le M_s, \tag{68}$$

$$|L_\tau(s, \tau)| \le M_\tau, |L_{ss}(s, \tau)| \le M_{ss}. \tag{69}$$

Then,

$$\begin{aligned}\|\chi\|_{L^2}^2 &= \int_0^1 \int_{-\pi}^{\pi} \left|\Xi(\theta, s) + \int_0^s L(s, \tau)\Xi(\theta, \tau)d\tau\right|^2 d\theta ds \\ &\le 2\|\Xi\|_{L^2}^2 + 2\int_0^1 \int_{-\pi}^{\pi} \left|\int_0^s L(s, \tau)\Xi(\theta, \tau)d\tau\right|^2 d\theta ds \\ &\le 2\|\Xi\|_{L^2}^2 + 2M^2 \int_0^1 \int_{-\pi}^{\pi} \int_0^s |\Xi(\theta, \tau)|^2 d\tau d\theta ds \\ &\le C_0 \|\Xi\|_{L^2}^2, \end{aligned} \tag{70}$$

where $C_0 = 2(1 + M^2)$.

We have

$$\begin{aligned}\chi_s(\theta, s) &= \Xi_s(\theta, s) + L(s, s)\Xi(\theta, s) + \int_0^s L_s(s, \tau)\Xi(\theta, \tau)d\tau, \\ \chi_\theta(\theta, s) &= \Xi_\theta(\theta, s) + \int_0^s L(s, \tau)\Xi_\theta(\theta, \tau)d\tau. \end{aligned} \tag{71}$$

Then, from the definition (62) of the H^1 norm on the cylindrical surface, we obtain

$$\begin{aligned}\|\chi\|_{H^1}^2 &= \|\chi\|_{L^2}^2 + \|\chi_s\|_{L^2}^2 + \|\chi_\theta\|_{L^2}^2 \\ &\le C_0\|\Xi\|_{L^2}^2 + 3\|\Xi_s\|_{L^2}^2 + 3M^2\|\Xi\|_{L^2}^2 + 3M_s^2\|\Xi\|_{L^2}^2 \\ &\quad + 2\|\Xi_\theta\|_{L^2}^2 + 2M^2\|\Xi_\theta\|_{L^2}^2 \\ &= (C_0 + 3M^2 + 3M_s^2)\|\Xi\|_{L^2}^2 + 3\|\Xi_s\|_{L^2}^2 \\ &\quad + 2(1 + M^2)\|\Xi_\theta\|_{L^2}^2 \\ &\le C_1\|\Xi\|_{H^1}^2, \end{aligned} \tag{72}$$

where

$$\begin{aligned}C_1 &= \max\left\{C_0 + 3M^2 + 3M_s^2, 3, 2 + 2M^2\right\} \\ &= \max\left\{2 + 5M^2 + 3M_s^2, 3\right\}. \end{aligned} \tag{73}$$

For the H^2 norm defined in (63), we have

$$\begin{aligned}\|\chi\|_{H^2}^2 &= \|\chi\|_{H^1}^2 + \int_0^1\int_{-\pi}^{\pi}(|\chi_{\theta\theta}|^2 + 2|\chi_{\theta s}|^2 + |\chi_{ss}|^2 \\ &\quad + |\chi_\theta|^2)d\theta ds \\ &\le C_1\|\Xi\|_{H^1}^2 + 2\|\Xi_{\theta\theta}\|_{L^2}^2 + 2M^2\|\Xi_{\theta\theta}\|_{L^2}^2 \\ &\quad + 6(M_s + M_\tau)\|\Xi\|_{L^2}^2 + 6M^2\|\Xi_s\|_{L^2}^2 \\ &\quad + 6M_{ss}^2\|\Xi\|_{L^2}^2 + 6M_s^2\|\Xi\|_{L^2}^2 + 2\|\Xi_\theta\|_{L^2}^2 \\ &\quad + 2M^2\|\Xi_\theta\|_{L^2}^2 + 6\|\Xi_{\theta s}\|_{L^2}^2 + 6M^2\|\Xi_\theta\|_{L^2}^2 \\ &\quad + 6M_s^2\|\Xi_\theta\|_{L^2}^2 \\ &= (C_1 + 6M_s^2 + 6M_\tau^2 + 6M_{ss}^2 + 6M_s^2)\|\Xi\|_{L^2}^2 \\ &\quad + (C_1 + 6M^2)\|\Xi_s\|_{L^2}^2 + C_1\|\Xi_\theta\|_{L^2}^2 + 6\|\Xi_{ss}\|_{L^2}^2 \\ &\quad + 2(1 + M^2)\|\Xi_{\theta\theta}\|_{L^2}^2 \\ &\quad + 2(1 + 4M^2 + 3M_s^2)\|\Xi_\theta\|_{L^2}^2 + 6\|\Xi_{\theta s}\|_{L^2}^2 \\ &\le C_2\|\Xi\|_{H^2}^2, \end{aligned} \tag{74}$$

where

$$\begin{aligned}C_2 = \max\big\{&C_1 + 6M_s^2 + 6M_\tau^2 + 6M_{ss}^2 + 6M_s^2, C_1 + 6M^2, \\ &6, 2\big(1 + 4M^2 + 3M_s^2\big)\big\}. \end{aligned} \tag{75}$$

■

Therefore, the original u-system and the transformed w-system are equivalent. Next we first discuss about the stability property of the w system.

Proposition 4.2: *For any initial condition $w(0, \theta, s) \in H^2(\Omega)$, the system (51)–(52) admits a (unique, mild) solution $w \in \mathcal{C}\left([0, \infty), H^2(\Omega)\right)$ and the equilibrium $w(t, \theta, s) \equiv 0$ is exponentially stable in the H^2 norm, in particular, there exist two constants $C_3 > 0$, $\alpha > 0$, such that*

$$\|w(t, \cdot)\|_{H^2} \le C_3 e^{-\alpha t}\|w(0, \cdot)\|_{H^2}. \tag{76}$$

Moreover, if the following boundary compatibility conditions

$$w(0, \theta, 0) = 0, w(0, \theta, 1) = 0 \tag{77}$$

are also satisfied, then the solution is classical.

Proof: The well-posedness result is standard (see, for instance, Brezis (2010)). For the norm estimates, consider first

$$V_1 = \frac{1}{2}\|w(t, \cdot)\|_{L^2}^2 = \frac{1}{2}\int_0^1\int_{-\pi}^{\pi}|w(t, \theta, s)|^2 d\theta ds. \tag{78}$$

Then,

$$\begin{aligned}\dot{V}_1 &= \int_0^1\int_{-\pi}^{\pi}\frac{ww_t^* + w^*w_t}{2}d\theta ds \\ &= \mathrm{Re}\int_0^1\int_{-\pi}^{\pi}\{w^*w_{ss} + w^*w_{\theta\theta}\}d\theta ds \\ &= -\int_0^1\int_{-\pi}^{\pi}\left(|w_s|^2 + |w_\theta|^2\right)d\theta ds, \end{aligned} \tag{79}$$

where w^* denotes the (complex) conjugate of w. To proceed, we employ the Poincare's inequality in cylindrical surface:

$$\int_0^1\int_{-\pi}^{\pi}|w|^2 d\theta ds \le 4\int_0^1\int_{-\pi}^{\pi}|w_s|^2 d\theta ds. \tag{80}$$

Then,

$$\dot{V}_1 \le -\frac{1}{4}\int_0^1\int_{-\pi}^{\pi}|w(t, \theta, s)|^2 d\theta ds = -\alpha_0 V_1, \tag{81}$$

where $\alpha_0 = 1/2$, and thus the L^2 norm stability of the system (51)–(52) is obtained. Take

$$V_2 = V_1 + \frac{1}{2}\int_0^1\int_{-\pi}^{\pi}(|w_s(t, \cdot)|^2 + |w_\theta(t, \cdot)|^2)d\theta ds, \tag{82}$$

which is equivalent to the square of the H^1 norm. Then,

$$\begin{aligned}\dot{V}_2 &= \dot{V}_1 + \frac{1}{2}\int_0^1\int_{-\pi}^{\pi}(w_s^*w_{st} + w_\theta^*w_{\theta t})d\theta ds \\ &= \dot{V}_1 - \int_0^1\int_{-\pi}^{\pi}|w_{ss} + w_{\theta\theta}|^2 d\theta ds \\ &\le -\int_0^1\int_{-\pi}^{\pi}\left(|w_s|^2 + |w_\theta|^2\right)d\theta ds \\ &\le -\frac{3}{8}V_1 - \frac{1}{4}\int_0^1\int_{-\pi}^{\pi}\left(|w_s|^2 + |w_\theta|^2\right)d\theta ds \\ &\le -\alpha_1 V_2, \end{aligned} \tag{83}$$

where $\alpha_1 = 3/8$. For the H^2 norm estimate, we define

$$V_3 = V_1 + V_2 + \frac{1}{2}\int_0^1\int_{-\pi}^{\pi}|\Delta w|^2 d\theta ds. \tag{84}$$

Note that

$$\begin{aligned}&\int_0^1\int_{-\pi}^{\pi}|w_{\theta s}|^2 d\theta ds \\ &= \frac{1}{2}\int_0^1\int_{-\pi}^{\pi}(w_{\theta\theta}w_{ss}^* + w_{\theta\theta}^*w_{ss})d\theta ds, \end{aligned} \tag{85}$$

then,

$$\frac{1}{2}\int_0^1\int_{-\pi}^{\pi}|\Delta w|^2 d\theta ds = \frac{1}{2}\int_0^1\int_{-\pi}^{\pi}(|w_{ss}|^2+|w_{\theta\theta}|^2+2|w_{\theta s}|^2)d\theta ds. \quad (86)$$

Hence, V_3 is equivalent to the square of the H^2 norm (63). Since $\Delta w = w_{ss} + w_{\theta\theta} = w_t$, we have the equation for Δw as: $(\Delta w)_t = \Delta(\Delta w)$ with $\Delta w(t, \theta, 0) = \Delta w(t, \theta, 1) = 0$. Note that this system is the same as (51), (52). Thus, Δw, treated as a state, is L^2 stable. Following a similar way as the previous development, it can be derived that $\dot{V}_3 \leq -\alpha V_3$, with $\alpha = 3/8$. From the equivalence between V_3 and the square of the H^2 norm, (76) can be proved. ■

From the equivalence between the original u-system and the transformed w-system, we obtain the following theorem stating that the designed feedback control law helps achieve exponential stability of the u-deployment profile in H^2 norm.

Theorem 4.1: *For any initial condition $u(0, \theta, s) \in H^2(\Omega)$, the closed-loop u-system (22), (24) with the control law (54) admits a (unique, mild) solution $u \in \mathcal{C}\left([0, \infty), H^2(\Omega)\right)$ that satisfies*

$$\|u(t, \cdot) - \bar{u}(\cdot)\|_{H^2} \leq Be^{-\alpha t}\|u(0, \cdot) - \bar{u}(\cdot)\|_{H^2} \quad (87)$$

for two constants $B > 0$ and $\alpha > 0$. Moreover, if $u(0, \theta, s)$ satisfies the boundary compatibility conditions

$$u(0, \theta, 0) = f_1(\theta), \quad (88)$$

$$u(0, \theta, 1) = \bar{u}(\theta, 1) - \int_0^1 \lambda\tau \frac{I_1\left[\sqrt{\lambda(1-\tau^2)}\right]}{\sqrt{\lambda(1-\tau^2)}} e^{-\frac{1}{2}\beta_1(1-\tau)} \times (u(0, \theta, \tau) - \bar{u}(\theta, \tau))d\tau, \quad (89)$$

then, the solution is classical.

A similar result could be obtained for the z system, and the details are omitted for simplicity. This obtained H^2 stability result guarantees that the neighbours in terms of the network topology remain neighbours in geometric space, which is important in practice to avoid the agents going out of the communication range.

5. Output feedback controller design

5.1 Observer design

The state feedback control law (54) assumes that each leader knows the positions of all the agents at all times, which is in general not realisable. Thus, we would like to design an observer to estimate these positions, using only measurement at the boundary, specifically, the derivative $u_s(t, \theta, 1)$. We propose the following observer:

$$\hat{v}_t(t, \theta, s) = \Delta\hat{v}(t, \theta, s) + \lambda\hat{v}(t, \theta, s) + P(t, \theta, s), \quad (90)$$

$$\hat{v}(t, \theta, 0) = 0, \quad (91)$$

$$\hat{v}(t, \theta, 1) = V(t, \theta) + p_{10}[v_s(t, \theta, 1) - \hat{v}_s(t, \theta, 1)], \quad (92)$$

where $\hat{v}(t, \theta, s)$ is the estimated state, $V(t, \theta)$ is the applied control (53), and the operators P, p_{10} are to be determined. Since the observer design is dual to the control design, it is foreseeable that the output injection operator P is independent of n. Then, we let

$$P(t, \theta, s) = p_1(s)\left(v_s(t, \theta, 1) - \hat{v}_s(t, \theta, 1)\right), \quad (93)$$

where $p_1(s)$ is the observer kernel gain.

To find the observer kernel $p_1(s)$ and the value p_{10} that guarantee convergence of $\hat{v}$ to v, we introduce the error variable $\tilde{v} = v - \hat{v}$, which satisfies

$$\tilde{v}_t(t, \theta, s) = \Delta\tilde{v}(t, \theta, s) + \lambda\tilde{v}(t, \theta, s) - p_1(s)\tilde{v}_s(t, \theta, 1), \quad (94)$$

$$\tilde{v}(t, \theta, 0) = 0, \quad (95)$$

$$\tilde{v}(t, \theta, s) = -p_{10}\tilde{v}_s(t, \theta, 1). \quad (96)$$

Proceeding as in Section 3, we consider the Fourier series expansion of $\tilde{v}(t, \theta, s)$, with the corresponding Fourier coefficients $\tilde{v}_n(t, s)$, respectively. Hence, we get a system of uncoupled equations for the $\tilde{u}_n$'s:

$$\tilde{v}_{nt}(t, s) = \tilde{v}_{nss}(t, s) - n^2\tilde{v}_n(t, s) + \lambda\tilde{v}_n(t, s) - p_1(s)\tilde{v}_{ns}(t, 1), \quad (97)$$

$$\tilde{v}_n(t, 0) = 0, \quad (98)$$

$$\tilde{v}_n(t, 1) = -p_{10}\tilde{v}_{ns}(t, 1). \quad (99)$$

We would like to transform each system (97) into a corresponding target system $\tilde{w}_n$ by using the mapping

$$\tilde{v}_n(t, s) = \tilde{w}_n(t, s) - \int_s^1 p(s, \tau)\tilde{w}_n(t, \tau)d\tau, \quad (100)$$

where the kernel $p(s,\tau)$ is defined on $\mathcal{T}_p = \{(s,\tau) : 0 \le s \le \tau \le 1\}$, and the desired target system is

$$\tilde{w}_{nt}(t,s) = \tilde{w}_{nss}(t,s) - n^2\tilde{w}_n(t,s),$$
$$\tilde{w}_n(t,0) = 0, \tag{101}$$

$$\tilde{w}_n(t,1) = 0. \tag{102}$$

Analogous to the controller design, we get the following observer kernel equation:

$$p_{ss} + p_{\tau\tau} = -\lambda p, \tag{103}$$

$$p(0,\tau) = 0, \tag{104}$$

$$p(s,s) = -\frac{\lambda}{2}s. \tag{105}$$

Solving the hyperbolic equations (103)–(105), we obtain

$$p(s,\tau) = -\lambda\tau\frac{\mathrm{I}_1\left[\sqrt{\lambda(\tau^2-s^2)}\right]}{\sqrt{\lambda(\tau^2-s^2)}}. \tag{106}$$

Moreover, the boundary conditions of the systems $\tilde{v}_n$, $\tilde{w}_n$ determine the observer gains:

$$p_1(s) = p(s,1) = -\lambda\frac{\mathrm{I}_1\left[\sqrt{\lambda(1-s^2)}\right]}{\sqrt{\lambda(1-s^2)}},\ p_{10} = 0 \tag{107}$$

Define a transformation from $\hat{v}$ to a new state $\hat{u}$ (which will serve as the observed state for u):

$$\hat{u}(t,\theta,s) = \bar{u}(\theta,s) + e^{-\frac{1}{2}\beta_1 s}\hat{v}(t,\theta,s), \tag{108}$$

then, we get the $\hat{u}$-system in the following explicit form:

$$\hat{u}_t(t,\theta,s) = \Delta\hat{u}(t,\theta,s) + \beta_1\hat{u}_s(t,\theta,s) + \lambda_1 u(t,\theta,s) - \lambda\frac{\mathrm{I}_1\left[\sqrt{\lambda(1-s^2)}\right]}{\sqrt{\lambda(1-s^2)}}\mathrm{e}^{\frac{1}{2}\beta_1(1-s)}(u_s(t,\theta,1) - \hat{u}_s(t,\theta,1)), \tag{109}$$

$$\hat{u}(t,\theta,0) = f_1(\theta), \tag{110}$$

$$\hat{u}(t,\theta,1) = g_1(\theta) - \int_0^1 \lambda\tau\frac{\mathrm{I}_1\left[\sqrt{\lambda(1-\tau^2)}\right]}{\sqrt{\lambda(1-\tau^2)}}\mathrm{e}^{-\frac{1}{2}\beta(1-\tau)} \times (\hat{u}(t,\theta,\tau) - \bar{u}(\theta,\tau))d\tau. \tag{111}$$

5.2 Output feedback stability

We now analyse the state stability in the H^2 norm of the output-feedback closed-loop $(u,\hat{u})$-system, where the u-system is composed of (3), (7), (8) with the following controller:

$$U(t,\theta) = -\int_0^1 \lambda\tau\frac{\mathrm{I}_1\left[\sqrt{\lambda(1-\tau^2)}\right]}{\sqrt{\lambda(1-\tau^2)}}\mathrm{e}^{-\frac{1}{2}\beta_1(1-\tau)} \times (\hat{u}(t,\theta,\tau) - \bar{u}(\theta,\tau))d\tau, \tag{112}$$

and the $\hat{u}$-system is (109)–(111). From (20) and (29), the u-system is equivalent to the v-system (30)–(32), with

$$V(t,\theta) = -\int_0^1 \lambda\tau\frac{\mathrm{I}_1\left[\sqrt{\lambda(1-\tau^2)}\right]}{\sqrt{\lambda(1-\tau^2)}}\hat{v}(t,\theta,\tau)d\tau. \tag{113}$$

Moreover, from (108), we can derive that the $\hat{u}$ system (109)–(111) is equivalent to the $\hat{v}$-system (90)–(92). Thus, the augmented $(u,\hat{u})$-system is equivalent to the $(v,\hat{v})$-system, and also equivalent to the $(\hat{v},\tilde{v})$-system. From the following two (smooth, invertible) mappings of state variables

$$\hat{w}(t,\theta,s) = \hat{v}(t,\theta,s) - \int_0^s K(s,\tau)\hat{v}(t,\theta,\tau)ds, \tag{114}$$

$$\tilde{v}(t,\theta,s) = \tilde{w}(t,\theta,s) - \int_s^1 p(s,\tau)\tilde{w}(t,\theta,\tau)ds, \tag{115}$$

the $(u,\hat{u})$-system is also equivalent to the resulting $(\hat{w},\tilde{w})$-system as follows:

$$\hat{w}_t(t,\theta,s) = \Delta\hat{w}(t,\theta,s) + \hat{F}(s)\tilde{w}(t,\theta,1), \tag{116}$$
$$\hat{w}(t,\theta,0) = \hat{w}(t,\theta,1) = 0, \tag{117}$$
$$\tilde{w}_t(t,\theta,s) = \Delta\tilde{w}(t,\theta,s), \tag{118}$$
$$\tilde{w}(t,\theta,0) = \tilde{w}(t,\theta,1) = 0, \tag{119}$$

where

$$\hat{F}(s) = p_1(s) - \int_0^s K_n(s,\tau)p_1(\tau)d\tau. \tag{120}$$

Obviously, we have that $\hat{F}(s) \in \mathcal{C}^\infty[0,1]$. While the H^2 stability of the origin for the $\tilde{w}$-system follows from Proposition 4.2, the stability of the cascade system is slightly more involved to prove. We first give a lemma as follows.

Lemma 5.1: *Suppose that $w(t,\theta,s)$ with $t>0$, $(\theta,s)\in\Omega$ is a complex-valued function satisfying*

$$w(t,\theta,0)=w(t,\theta,1)=0, \tag{121}$$

then,

$$\int_{-\pi}^{\pi}|w_s(t,\theta,1)|^2d\theta\le 3\int_0^1\int_{-\pi}^{\pi}|w_{ss}(t,\theta,s)|^2d\theta ds. \tag{122}$$

Proof: Through integration by parts, we get

$$\begin{aligned}&\int_0^1\int_{-\pi}^{\pi}s\left(w_s^*w_{ss}+w_sw_{ss}^*\right)d\theta ds\\&=\int_{-\pi}^{\pi}|w_s(t,\theta,1)|^2d\theta\\&\quad-\int_0^1\int_{-\pi}^{\pi}|w_s(t,\theta,s)|^2d\theta ds.\end{aligned} \tag{123}$$

That is,

$$\begin{aligned}&\int_{-\pi}^{\pi}|w_s(t,\theta,1)|^2d\theta\\&=\int_0^1\int_{-\pi}^{\pi}|w_s(t,\theta,s)|^2d\theta ds\\&\quad+2\mathrm{Re}\left\{\int_0^1\int_{-\pi}^{\pi}sw_s^*w_{ss}d\theta ds\right\}.\end{aligned} \tag{124}$$

By Cauchy–Schwarz and Young's inequalities, it holds that

$$\begin{aligned}&\int_{-\pi}^{\pi}|w_s(t,\theta,1)|^2d\theta\\&\le\int_0^1\int_{-\pi}^{\pi}|w_s(t,\theta,s)|^2d\theta ds\\&\quad+2\int_0^1\int_{-\pi}^{\pi}|w_{ss}(t,\theta,s)|^2d\theta ds\\&\le 3\int_0^1\int_{-\pi}^{\pi}|w_{ss}(t,\theta,s)|^2d\theta ds,\end{aligned} \tag{125}$$

where we have used the Poincare's inequality

$$\int_0^1\int_{-\pi}^{\pi}|w_s(t,\theta,s)|^2d\theta ds\le\int_0^1\int_{-\pi}^{\pi}|w_{ss}(t,\theta,s)|^2d\theta ds,$$

which was stated in Lemma 3.1 of Vázquez et al. (2008). ■

We obtain next the following result.

Proposition 5.1: *For any initial conditions $\hat{w}(0,\theta,s),\tilde{w}(0,\theta,s)\in H^3(\Omega)$, there exist constants B_1, $\alpha_4>0$ such that the system (116)–(119) admits a (unique, mild) solution $\hat{w},\tilde{w}\in\mathcal{C}\left([0,\infty),H^2(\Omega)\right)$ satisfying*

$$\begin{aligned}&\|\hat{w}(t,\cdot)\|_{H^2}+\|\tilde{w}(t,\cdot)\|_{H^2}\\&\le B_1\mathrm{e}^{-\alpha_4 t}\left(\|\hat{w}(0,\cdot)\|_{H^2}+\|\tilde{w}(0,\cdot)\|_{H^2}\right).\end{aligned} \tag{126}$$

Moreover, if the boundary compatibility conditions

$$\hat{w}(0,\theta,0)=0,\ \hat{w}(0,\theta,1)=0, \tag{127}$$

$$\tilde{w}(0,\theta,0)=0,\ \tilde{w}(0,\theta,1)=0, \tag{128}$$

are satisfied, then the solution is classical.

Proof: Due to the presence of $\tilde{w}_s(t,\theta,1)$ in (116), one needs the H^1 norm of $\tilde{w}$ to deduce the L^2 stability of $\hat{w}$, so we begin with the H^1 analysis. Take

$$\begin{aligned}V_1=&\frac{1}{2}\|\hat{w}\|_{L^2}^2+\frac{1}{2}\|\tilde{w}\|_{L^2}^2+\frac{1}{2}\|\hat{w}_\theta\|_{L^2}^2+\frac{1}{2}\|\hat{w}_s\|_{L^2}^2\\&+\frac{A_1}{2}\|\tilde{w}_\theta\|_{L^2}^2+\frac{A_1}{2}\|\tilde{w}_s\|_{L^2}^2,\end{aligned} \tag{129}$$

where $A_1>0$. One can easily derive that V_1 is equivalent to the square of the H^1 norm of the cascade $(\hat{w},\tilde{w})$-system state. By differentiating V_1 and integrating by parts, we find

$$\begin{aligned}\dot{V}_1=&\frac{1}{2}\int_0^1\int_{-\pi}^{\pi}\hat{w}^*\hat{w}_t+\tilde{w}^*\tilde{w}_t+\hat{w}_s^*\hat{w}_{st}+\hat{w}_\theta^*\hat{w}_{\theta t}\\&+A_1\tilde{w}_s^*\tilde{w}_{st}+A_1\tilde{w}_\theta^*\tilde{w}_{\theta t}d\theta ds\\=&-\int_0^1\int_{-\pi}^{\pi}\left(|\hat{w}_s|^2+|\hat{w}_\theta|^2\right)d\theta ds\\&-\int_0^1\int_{-\pi}^{\pi}\left(|\tilde{w}_s|^2+|\tilde{w}_\theta|^2\right)d\theta ds\\&-\int_0^1\int_{-\pi}^{\pi}|\hat{w}_{ss}+\hat{w}_{\theta\theta}|^2d\theta ds\\&-A_1\int_0^1\int_{-\pi}^{\pi}|\tilde{w}_{ss}+\tilde{w}_{\theta\theta}|^2d\theta ds\\&+\mathrm{Re}\left\{\int_0^1\int_{-\pi}^{\pi}(\hat{w}^*(t,\theta,s)-\Delta\hat{w}^*(t,\theta,s))\right.\\&\left.\times\hat{F}(s)\tilde{w}_s(\theta,1)d\theta ds\right\}.\end{aligned} \tag{130}$$

By using the Cauchy–Schwarz inequality, Young's inequality, Poincare's inequality (80) and Lemma 5.1,

we obtain

$$\begin{aligned}\dot{V}_1 \le & -\int_0^1\int_{-\pi}^{\pi}\left(|\hat{w}_s|^2+|\hat{w}_\theta|^2\right)d\theta ds\\ & -\int_0^1\int_{-\pi}^{\pi}\left(|\tilde{w}_s|^2+|\tilde{w}_\theta|^2\right)d\theta ds\\ & -\int_0^1\int_{-\pi}^{\pi}|\hat{w}_{ss}+\hat{w}_{\theta\theta}|^2 d\theta ds\\ & -A_1\int_0^1\int_{-\pi}^{\pi}|\tilde{w}_{ss}+\tilde{w}_{\theta\theta}|^2 d\theta ds\\ & +\frac{1}{2\gamma}\int_0^1\int_{-\pi}^{\pi}(|\hat{w}|^2+|\Delta\hat{w}|^2)\theta ds\\ & +\frac{\gamma}{2}\int_0^1\int_{-\pi}^{\pi}|\hat{F}(s)\tilde{w}_s(t,\theta,1)|^2 d\theta ds\\ \le & -\left(\frac{1}{8}-\frac{1}{2\gamma}\right)\|\hat{w}\|_{L^2}^2-\frac{1}{8}\|\tilde{w}\|_{L^2}^2\\ & -\frac{1}{2}\left(\|\hat{w}_s\|_{L^2}^2+\|\tilde{w}_s\|_{L^2}^2\right)-\left(\|\hat{w}_\theta\|_{L^2}^2+\|\tilde{w}_\theta\|_{L^2}^2\right)\\ & -\left(1-\frac{1}{2\gamma}\right)\|\Delta\hat{w}\|_{L^2}^2-\left(A_1-\frac{3}{2}\gamma G^2\right)\|\tilde{w}_{ss}\|_{L^2}^2\\ & -A_1\left(\|\tilde{w}_{\theta\theta}\|_{L^2}^2+2\|\tilde{w}_{\theta s}\|_{L^2}^2\right),\end{aligned}\tag{131}$$

where $\gamma>0$ is an arbitrary positive constant; the following equation

$$\begin{aligned}&\int_0^1\int_{-\pi}^{\pi}\left(\frac{1}{2}\tilde{w}_{ss}\tilde{w}_{\theta\theta}^*+\frac{1}{2}\tilde{w}_{ss}^*\tilde{w}_{\theta\theta}\right)d\theta ds\\ &\quad=\int_0^1\int_{-\pi}^{\pi}|\tilde{w}_{\theta s}|^2 d\theta ds,\end{aligned}\tag{132}$$

is derived from the homogenous boundary conditions and is used in the second inequality, and we assume $|\hat{F}(s)|\le G$, since $\hat{F}(s)\in\mathcal{C}^\infty[0,1]$. Let $\gamma>4$, $A_1>\frac{3}{2}\gamma G^2$, then we obtain

$$\dot{V}_1\le\alpha_3 V_1,\tag{133}$$

where $\alpha_3=\min\{\frac{1}{8}-\frac{1}{2\gamma},\frac{1}{2A_1}\}>0$.

Consider

$$V_2=V_1+\frac{1}{2}\|\Delta\hat{w}\|_{L^2}^2+\frac{A_2}{2}\|\Delta\tilde{w}\|_{L^2}^2,\tag{134}$$

where $A_2>0$. It is also obvious that V_2 is equivalent to the square of the H^2 norm. Take the time derivative

$$\begin{aligned}\dot{V}_2=\dot{V}_1-&\int_0^1\int_{-\pi}^{\pi}(|\Delta(\hat{w}_s)|^2+|\Delta(\hat{w}_\theta)|^2+A_2|\Delta(\tilde{w}_s)|^2\\ &+A_2|\Delta(\tilde{w}_s)|^2)d\theta ds+\int_0^1\int_{-\pi}^{\pi}\Delta\hat{w}\Delta(\hat{F}(s)\\ &\times\tilde{w}_s(t,\theta,1))d\theta ds.\end{aligned}\tag{135}$$

We have

$$\tilde{w}_{\theta t}(t,\theta,s)=\tilde{w}_{\theta ss}(t,\theta,s)+\tilde{w}_{\theta\theta\theta}(t,\theta,s),\tag{136}$$

$$\tilde{w}_\theta(t,\theta,0)=\tilde{w}_\theta(t,\theta,1)=0.\tag{137}$$

The above system has the same form as the $\tilde{w}$ system and thus has a similar property:

$$\int_{-\pi}^{\pi}|\tilde{w}_{\theta s}(t,\theta,1)|^2 d\theta\le 3\int_0^1\int_{-\pi}^{\pi}|\tilde{w}_{\theta ss}(t,\theta,s)|^2 d\theta ds.\tag{138}$$

Therefore, the last term of (135) becomes

$$\begin{aligned}&\int_0^1\int_{-\pi}^{\pi}\Delta\hat{w}\Delta(\hat{F}(s)\tilde{w}_s(t,\theta,1))d\theta ds\\ &=\int_0^1\int_{-\pi}^{\pi}\Delta\hat{w}(\hat{F}_{ss}\tilde{w}_s(t,\theta,1)+\hat{F}(s)\tilde{w}_{s\theta\theta}(t,\theta,1))d\theta ds\\ &=\int_0^1\int_{-\pi}^{\pi}\Delta\hat{w}\hat{F}_{ss}\tilde{w}_s(t,\theta,1)\\ &\quad-\Delta(\hat{w}_\theta)\hat{F}(s)\tilde{w}_{s\theta}(t,\theta,1))d\theta ds\\ &\le\int_0^1\int_{-\pi}^{\pi}\left[\frac{1}{2\gamma}(|\Delta\hat{w}|^2+|\Delta(\hat{w}_\theta)|^2)\right.\\ &\quad\left.+\frac{1}{2}\gamma\left(G_{ss}^2|\tilde{w}_s(t,\theta,1)|^2+G^2|\tilde{w}_{\theta s}(t,\theta,1)|^2\right)\right]d\theta ds\\ &\le\int_0^1\int_{-\pi}^{\pi}\left[\frac{1}{2\gamma}(|\Delta\hat{w}|^2+|\Delta(\hat{w}_\theta)|^2)\right.\\ &\quad\left.+\frac{3}{2}\gamma\left(G_{ss}^2|\tilde{w}_{ss}|^2+G^2|\tilde{w}_{\theta ss}|^2\right)\right]d\theta ds.\end{aligned}\tag{139}$$

By Cauchy–Schwarz, Young's, and Poincaré's inequalities, we find

$$\begin{aligned}\dot{V}_2\le & -\alpha_3 V_1-\left(1-\frac{1}{2\gamma}\right)\|\Delta\hat{w}\|_{L^2}^2-\left(A_1-\frac{3}{2}\gamma G^2\right)\\ & \times\|\tilde{w}_{ss}\|_{L^2}^2-A_1\left(\|\tilde{w}_{\theta\theta}\|_{L^2}^2+2\|\tilde{w}_{\theta s}\|_{L^2}^2\right)\\ & -\|\Delta(\hat{w}_s)\|_{L^2}^2-\|\Delta(\hat{w}_\theta)\|_{L^2}^2-A_2(\|\Delta(\tilde{w}_s)\|_{L^2}^2\\ & +\|\Delta(\tilde{w}_\theta)\|_{L^2}^2)+\frac{1}{2\gamma}\left(\|\Delta\hat{w}\|_{L^2}^2+\|\Delta(\hat{w}_\theta)\|_{L^2}^2\right)\\ & +\frac{3}{2}\gamma\left(G_{ss}^2\|\tilde{w}_{ss}\|_{L^2}^2+G^2\|\tilde{w}_{\theta ss}\|_{L^2}^2\right)\\ \le & -\alpha_3 V_1-\left(1-\frac{1}{\gamma}\right)\|\Delta\hat{w}\|_{L^2}^2-\left(A_1-\frac{3}{2}\gamma G^2\right.\\ & \left.-\frac{3}{2}\gamma G_{ss}^2\right)\|\tilde{w}_{ss}\|_{L^2}^2-A_1\left(\|\tilde{w}_{\theta\theta}\|_{L^2}^2+2\|\tilde{w}_{\theta s}\|_{L^2}^2\right)\end{aligned}$$

$$
\begin{aligned}
&-\|\Delta(\hat{w}_s)\|_{L^2}^2-\left(1-\frac{1}{2\gamma}\right)\|\Delta(\hat{w}_\theta)\|_{L^2}^2\\
&-A_2\left(\|\Delta(\tilde{w}_s)\|_{L^2}^2+\|\tilde{w}_{\theta\theta\theta}\|_{L^2}^2+2\|\tilde{w}_{\theta\theta s}\|_{L^2}^2\right)\\
&-\left(A_2-\frac{3}{2}\gamma G^2\right)\|\tilde{w}_{\theta ss}\|_{L^2}^2. \qquad (140)
\end{aligned}
$$

Let $A_1 > \frac{3}{2}\gamma(G^2+G_{ss}^2)$ and $A_2 > \frac{3}{2}\gamma G^2$, we reach

$$\dot{V}_2 \le -\alpha_4 V_2, \qquad (141)$$

where $\alpha_4 = \min\{\alpha_3, A_1 - \frac{3}{2}\gamma(G^2+G_{ss}^2)\} > 0$. Thus, the proposition is proved. ■

From the equivalence between the $(u,\hat{u})$-system and the $(\hat{w},\tilde{w})$-system, after some calculations, we could arrive at the following main result.

Theorem 5.1: *For any initial conditions $u_0(\theta, s)$, $\hat{u}_0(\theta, s) \in H^3(\Omega)$, there exist constants $D, \alpha_o > 0$ such that the augmented $(u,\hat{u})$-system of the u-system (3), (7), (8), (112) and the $\hat{u}$-system (109)–(111) admit a (unique, mild) solution $(u,\hat{u}) \in C\left([0,\infty), H^2(\Omega)\right)$ and*

$$
\begin{aligned}
&\|u(t,\cdot)-\bar{u}(\cdot)\|_{H^2}+\|\hat{u}(t,\cdot)-\bar{u}(\cdot)\|_{H^2}\\
&\quad\le De^{-\alpha_o t}\left(\|u_0-\bar{u}(\cdot)\|_{H^2}+\|\hat{u}_0-\bar{u}(\cdot)\|_{H^2}\right). \qquad (142)
\end{aligned}
$$

Moreover, if the compatibility conditions

$$
\begin{aligned}
&u(0,\theta,0) = f_1(\theta), \qquad (143)\\
&\hat{u}(0,\theta,0) = f_1(\theta), \qquad (144)\\
&u(0,\theta,1) = g_1(\theta) - \int_0^1 \lambda\tau \frac{I_1\left[\sqrt{\lambda(1-\tau^2)}\right]}{\sqrt{\lambda(1-\tau^2)}} e^{-\frac{1}{2}\beta(1-\tau)}\\
&\qquad\times(\hat{u}(0,\theta,\tau)-\bar{u}(\theta,\tau))d\tau, \qquad (145)\\
&\hat{u}(0,\theta,1) = g_1(\theta) - \int_0^1 \lambda\tau \frac{I_1\left[\sqrt{\lambda(1-\tau^2)}\right]}{\sqrt{\lambda(1-\tau^2)}} e^{-\frac{1}{2}\beta(1-\tau)}\\
&\qquad\times(\hat{u}(0,\theta,\tau)-\bar{u}(\theta,\tau))d\tau \qquad (146)
\end{aligned}
$$

are satisfied, then the solution is classical.

A similar result also holds for the real-valued system of $z(t,\theta,s)$.

6. Numerical simulations

6.1 Discretised agent control laws

In order to apply the feedback control laws to the multi-agent systems, we discretise the PDE model (3)–(4) in the space Ω by

$$\theta_i = (i-1)h_\theta, \quad s_j = (j-1)h_s \quad i = \overline{1,N},\ j = \overline{1,M}, \qquad (147)$$

where $h_\theta = \frac{2\pi}{N-1}$, $h_s = \frac{1}{M-1}$. The following three-point central difference approximation[1] of (3)–(4) is considered:

$$
\begin{aligned}
\dot{u}_{i,j} &= \frac{u_{i+1,j}-2u_{i,j}+u_{i-1,j}}{h_\theta^2} + \frac{u_{i,j+1}-2u_{i,j}+u_{i,j-1}}{h_s^2}\\
&\quad+\beta_1\frac{u_{i+1,j}-u_{i-1,j}}{2h_s}+\lambda_1 u_{i,j}, \qquad (148)\\
\dot{z}_{i,j} &= \frac{z_{i+1,j}-2z_{i,j}+z_{i-1,j}}{h_\theta^2} + \frac{z_{i,j+1}-2z_{i,j}+z_{i,j-1}}{h_s^2}\\
&\quad+\beta_2\frac{z_{i+1,j}-z_{i-1,j}}{2h_s}+\lambda_2 z_{i,j} \qquad (149)
\end{aligned}
$$

for the follower agents (i,j) with $i = \overline{1,N-1}$, $j = \overline{2,M-1}$. Both the state variables u, z are 2π-periodic in θ, which gives $u_{1,j} = u_{N,j}$ and $z_{1,j} = z_{N,j}$. For the leader agents at $j = 1$, we have

$$u_{i,1} = f(\theta_i) \triangleq f_i. \qquad (150)$$

For the leader agents at $j = M$, we have

$$u_{i,M} = g_i + \sum_{j=1}^{M} K_j a_j (u_{i,j} - \bar{u}_{i,j}), \qquad (151)$$

which gives the following actuation law:

$$u_{i,M} = g_i + \frac{1}{1-K_M a_M}\sum_{j=1}^{M-1} K_j a_j (u_{i,j} - \bar{u}_{i,j}), \qquad (152)$$

where g_i's, $\bar{u}_{i,j}$'s denote the desired formation, $u_{i,j}$'s are the actual positions served as the state feedback, and $K_j = -\lambda s_j \frac{I_1\sqrt{\lambda(1-s_j^2)}}{\sqrt{\lambda(1-s_j^2)}}$ is the discretised control kernel for u. The coefficients a_j are determined by the Simpson's rules of numerical integration,

$$
\begin{aligned}
&a_j = \frac{1}{3},\ \{j = 1, M\};\\
&a_j = \frac{4}{3},\ \{j = 2, 4, \ldots, M-1\};\\
&a_j = \frac{2}{3},\ \{j = 3, 5, \ldots, M-2\}; \qquad (153)
\end{aligned}
$$

where M has to be chosen as odd numbers according to Simpson's rules. Similar formula can also be obtained for z.

In practice, we use the estimated values for $u_{i,j}$, which are derived by running the observer on the actuation leaders' central processing unit (CPU). The observer only requires one boundary measurement $u_s(t, \theta, 1)$, which can be approximated through some finite-difference schemes. For example, it is possible for the leader to only measure the position of the nearest neighbour by using a one-sided expression $u_s(t, \theta, 1) = \frac{1}{h_s}(u_{i,M} - u_{i,M-1})$, which has a discretisation error $\mathcal{O}(h_s)$. Here, we use a second-order accurate approximation of the observer variable (see LeVeque, 2007)

$$u_s(t, \theta, 1) = \frac{3}{2h_s}u_{i,M} - \frac{2}{h_s}u_{i,M-1} + \frac{1}{2h_s}u_{i,M-2}. \tag{154}$$

Hence, each actuation leader (i, M) needs to measure the positions of its nearest neighbour and the second nearest neighbour. The approximating error coming from the discretisation process is now $O(h_s^2 + h_\theta^2)$. Indeed, higher order approximations could also help reduce the error, with a price of increasing the complexity of both the communication network and the controller. Moreover, since an increase in the number of agents would (greatly) decrease the error, the PDE-based method is quite suitable for analysing large-scale systems.

6.2 Numerical simulations for the discretised agent control laws

In order to show the effectiveness of the distributed control laws, we conduct some simulations for the formation control of a system of 81 × 90 agents on a mesh-grid in the 3-D space, with the parameters $\lambda_1 = 30$, $\beta_2 = 0$. The output-feedback control law is designed, which uses the estimates of the full states through an observer, and the initial conditions for the observer are all set to be zero.

By changing the positions of the leader agents according to the boundary conditions, the agent formations can transit from one desired manifold to another. More specifically, we force the agents to transit along three formations manifolds: starting from a manifold with a circular boundary where $f_1(\theta) = g_1(\theta) = e^{j\theta}$, $f_2(\theta) = 0$, $g_2(\theta) = 1$, and $\beta_1 = 1 + 3j$, $\lambda_2 = 24$, through a manifold with a parametric boundary where $f_1(\theta) = g_1(\theta) = e^{j\theta} - e^{3j\theta}$, $f_2(\theta) = g_2(\theta) = 1$, and $\beta_1 = 0$, $\lambda_2 = 18$ and finally settling to a manifold with a Lissajous boundary where $f_1(\theta) = g_1(\theta) = \frac{1}{2}e^{-3j\theta} - \frac{1}{2}e^{-2j\theta} + \frac{1}{2}e^{2j\theta} + \frac{1}{2}e^{3j\theta}$, $f_2(\theta) = g_2(\theta) = 1$, and $\beta_1 = 0, \lambda_2 = 18$. A video of the simulation results can be downloaded from Qi (2016). For the readers' convenience, we also show several snapshots of the simulation in Figure 3. To avoid producing undesirable large transients during a short time of transiting, we use a continuous, slowly varying formation to connect each pair of consecutive formation patterns. This allows the leaders on the boundary to change positions slowly. The left insets in each sub-figure of Figure 3 show different evolution stages of the reference formation of leaders, and the right insets show the corresponding actual formation of the leaders. Specifically, the insets on the upper-left corners of the sub-figures in Figure 3 show the reference formation (dashed green line) on which the leaders with $j = 1$ and $i = \overline{1, N}$ deploy, and those on the lower-left corners are the reference formation (dashed orange line) for the leaders with $j = M$ and $i = \overline{1, N}$. The insets on the upper-right corners demonstrate the actual shapes (solid green line) formed by the leaders, and the insets on the lower-right corner (solid orange line) are the actual shapes formed by the leaders. As shown in Figure 3, the actual formations change even slower than the reference formations. In particular, as shown in (d) and (h) of Figure 3, the actual leaders successfully converge to the reference. Since the system behaves as a diffusion process, in practice, the reference signals are propagated from the boundary to the formation centre, eventually forcing all agents to reach the desired formation.

We also plot the observed errors between the estimated states and the actual states, and the tracking errors between the reference formation and the actual one in Figure 4(a,b), respectively. More precisely, the agents' tracking errors at different layers, namely $i = 3$, $i = 41$, and $i = 72$, are shown, as well as the errors of the actuation leaders and the average error for all the agents. It can be seen that it only takes about 0.6 seconds for the observer errors to settle down uniformly (close to zero). The tracking errors converge slower. At formation transitions, the tracking errors increase suddenly; and when the reference stops changing, they converge (fast) again back to zero. Moreover, the errors at the upper layer such as $i = 3$ is smallest because they are closer to and thus quickly follows the desired formation. It can also be noticed that the mean error of all the agents is smaller than the mean error of the leaders. This is reasonable because the leaders play the role of driving the whole system besides their own formation control. The averaged control efforts U and Z over all the leaders are shown in Figure 4(c), which are bounded and have a similar varying trend to the tracking errors. Control effort Z remains unchanged for the second formation transition because the desired formation along the height coordinate keeps unchanged after the first transition.

Furthermore, we study the collisions among the agents during the evolution by numerical simulations. Idealising the agents as mass points and considering a non-collision

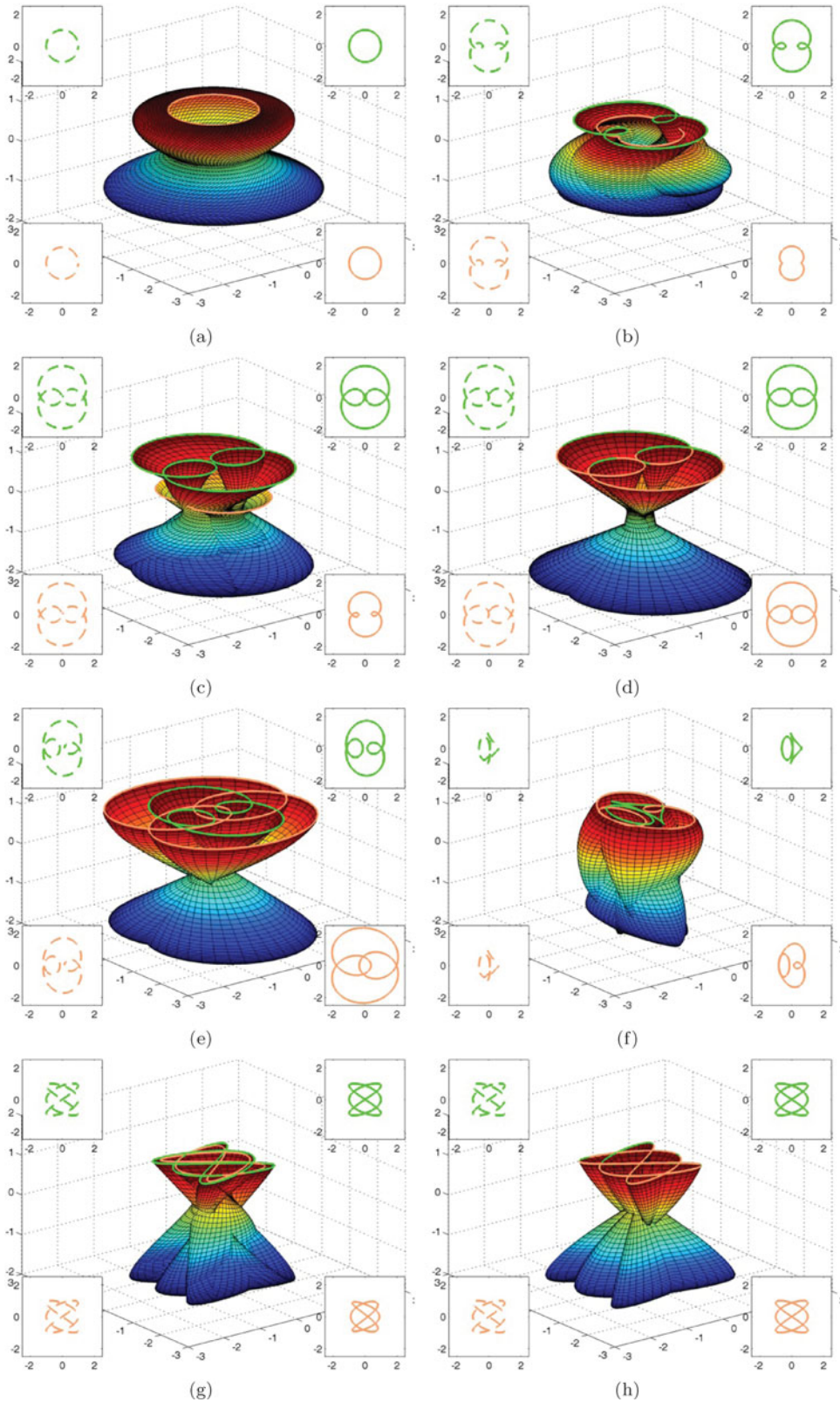

Figure 3. Agents formation transition snapshots. The left insert of each diagram represents the desired formation of the leaders and the right insert represents the actual position of the leaders. The green curves (also shown in upper right insert) denote the formation shapes for leaders $j = 1$ and $i = \overline{1, N}$, while the orange curves (also shown in bottom right insert) represent the shapes for leaders' $j = M$ and $i = \overline{1, N}$. The formation begins with a circle pattern (a), transits through the intermediate stages (b), (c), and arrives at the parametric curve pattern (d). Then, the formation changes from the pattern (d) to finally settle in the Lissajous pattern (h), through the transient intermediate stages (e), (f) and (g).

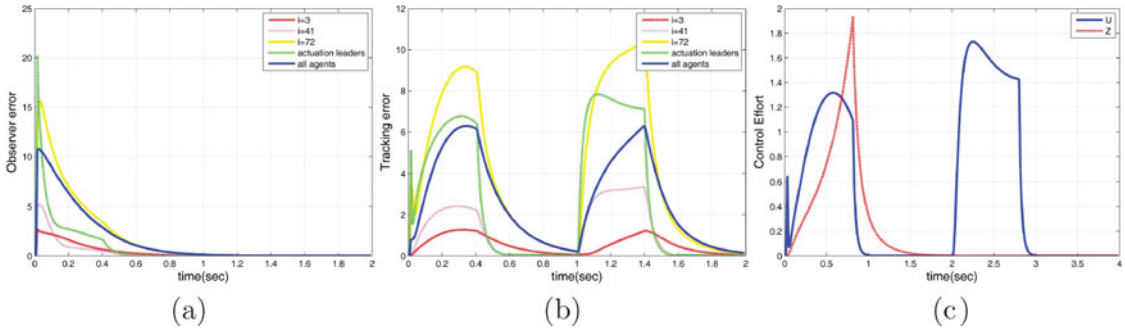

Figure 4. Agents tracking error and observer error during the simulation. (a) Observer error between the actual position and the estimated one. (b) Tracking error between the actual formation and the reference manifold. (c) The averaged control efforts U and Z over the entire leaders.

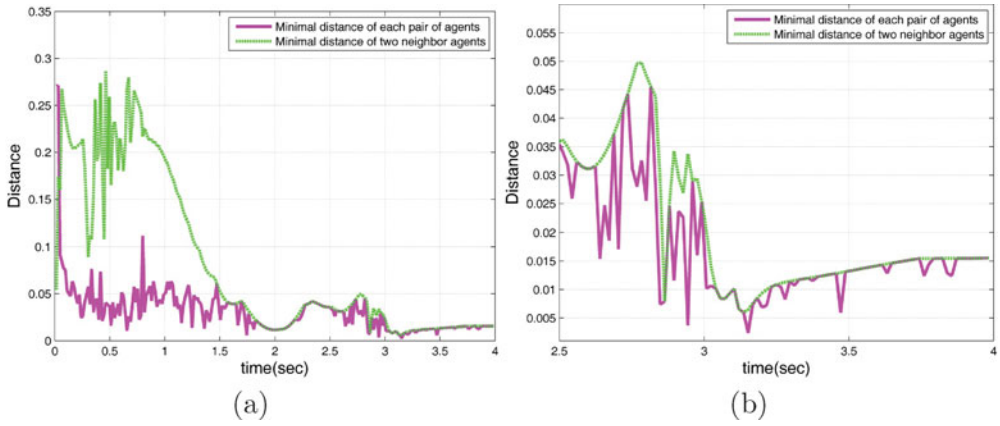

Figure 5. (a) The minimal distance of each pair of agents and the minimal distance between two neighbouring agents from time 0 to 4s. (b) The same distances from time 2.5 to 4s which is for more clearly illustration.

initial formations of the agents, it is shown from Figure 5 that the minimal distance (in the 3-D space) of any pair of agents over time is non-zero. Note that there are 7290 agents within a space of $(-3, 3) \times (-3, 3) \times (-2, 1)$ and the minimal distances may be bigger if the desired formation is enlarged. Suppose that the distance unit is metre, as defined above, each agent averagely occupies 0.0025 m^3 at most, as thus the minimal distance over time in Figure 5 is 0.0024 m which could be the normal distance so there is no collision occurring in our numerical examples. We have also conducted the similar check for all the other simulations with different desired formation considered in this paper, and do not find collisions among the agents. This collision avoidance among agents may be possible due to no collision either for the initial conditions or for the final equilibriums. However, besides the intuitive check from the simulation point of view, more deep and strict analysis and investigation are needed to derive a systematic and reliable conclusion.

7. Conclusions

In this paper, we introduce a distributed framework for the multi-agent formation control on a 2-D cylindrical surface in the 3-D space, by employing a PDE-based model for the agents. Boundary controllers are designed for the PDE model, which corresponds to a leader-enabled mode. The stability of the resulting closed-loop PDE system with respect to the H^2 norm guarantees the agents that are adjacent to each other on the topology are also neighbours in the physical space. Note that there are usually limitations on each agent in its physical communication range. Since our control law only requires each agent to obtain local information from the neighbours on the topology, instead of the global information from all the agents, this relaxation increases the practical value of this method.

The discretisation of the spatial derivatives of the PDE determines the control laws for the follower agents, while

the boundary conditions determine the control laws actuated by the leader agents. Based on the designed boundary observer which recovers the positions of all the agents from one boundary measurement, each agent, either a leader or a follower, requires only information from its neighbours, which results in a distributed scheme.

Collision among the agents is an important and interesting problem. In the numerical simulation examples presented in this paper, no collision occurs. For further research, one could analyse whether the proposed method implies a collision avoidance scheme and if not, how to guarantee that no collision occurs. Another future possible research topics include the extension of this paradigm to the formation tracking control, that is, to make the agents move along a target orbit and also keep the desired formation. Recall that the model in this paper corresponds to coupled first-order integrators; thus, one intriguing line of research would be to employ a wave-like PDE to model the second-order integrator, namely, the acceleration control, which will increase potential applications. In addition, the robustness of the designed controllers for the multi-agent systems with disturbance or input delay is worth considering

Note

1. A more flexible approach based on multi-indices can be found in Meurer (2013), which increases the number of possible underlying graph topologies. In this paper, we limit ourselves to the three-point central difference scheme for the sake of simplicity.

Disclosure statement

No potential conflict of interest was reported by the authors.

Funding

National Natural Science Foundation of China [grant number 61134009, 61473265]; Natural Science Foundation of Shanghai [16ZR1401200]; Fundamental Research Funds for the Central Universities [2232015D3-24].

References

Barooah, P., Mehta, P.G., & Hespanha, J.P. (2009). Mistuning-based control design to improve closed-loop stability margin of vehicular platoons. *IEEE Transactions on Automatic Control*, *54*(9), 2100–2113.

Blondel, V.D., Hendrickx, J.M., & Tsitsiklis, J.N. (2010). Continuous-time average-preserving opinion dynamics with opinion-dependent communications. *SIAM Journal on Control and Optimization*, *48*(8), 5214–5240.

Brezis, H. (2010). *Functional analysis, Sobolev spaces and partial differential equations*. New York City: Springer.

Bullo , F., Cortés, J., & Martinez, S. (2009). Distributed control of robotic networks: A mathematical approach to motion coordination algorithms. Princeton, NJ: Princeton University Press.

Canuto, C., Fagnani, F., & Tilli, P. (2008). An Eulerian approach to the analysis of rendezvous algorithms , In *Proceedings of 17th IFAC World Conference*, Seoul, South Korea: IFAC (pp. 9039–9044).

Cao, Y., Yu, W., Ren, W., & Chen, G. (2013). An overview of recent progress in the study of distributed multi-Agent coordination. *IEEE Transactions on Industrial Informatics*, *9*(1), 427–438.

Dasdemir, J., & Loría, A. (2014). Robust formation tracking control of mobile robots via one-to-one time-varying communication. *International Journal of Control*, *87*(9), 1822–1832.

Dunbabin, M., & Marques, L. (2012). Robots for environmental monitoring: Significant advancements and applications. *IEEE Robotics Automation Magazine*, *19*(1), 24–39.

Ferrari-Trecate, G., Buffa, A., & Gati, M. (2006). Analysis of coordination in multi-agent systems through partial difference equations. *IEEE Transactions on Automatic Control*, *51*(6), 1058–1063.

Frihauf, P., & Krstic, M. (2011). Leader-enabled deployment onto planar curves: A PDE-based approach. *IEEE Transactions on Automatic Control*, *56*(8), 1791–1806.

Ghods, N., & Krstic, M. (2012). Multi-agent deployment over a source. *IEEE Transactions on Control Systems Technology*, *20*(1), 277–285.

Han, J., Xu, Y., Di, L., & Chen, Y. (2013). Low-cost multi-UAV technologies for contour mapping of nuclear radiation field. *Journal of Intelligent & Robotic Systems*, *70*(1–4), 401–410.

Hao, H., & Barooah, P. (2012). Approximation error in PDE-based modelling of vehicular platoons. *International Journal of Control*, *85*(8), 1121–1129.

Hao, H., Barooah, P., & Mehta, P.G. (2011). Stability margin scaling laws for distributed formation control as a function of network structure. *IEEE Transactions on Automatic Control*, *56*(4), 923–929.

Hatanaka, T., Chopra, N., Fujita, M., & Spong, M.W. (2015). *Passivity-based control and estimation in networked robotics*, Springer.

Helbing, D. (2001). Traffic and related self-driven many-particle systems. *Reviews of Modern Physics*, *73*(4), 1067.

Kalantar, S., & Zimmer, U.R. (2007). Distributed shape control of homogeneous swarms of autonomous underwater vehicles. *Autonomous Robots*, *22*(1), 37–53.

Kim, J., Kim, K.D., Natarajan, V., Kelly, S.D., & Bentsman, J. (2008). PdE-based model reference adaptive control of uncertain heterogeneous multi-agent networks. *Nonlinear Analysis: Hybrid Systems*, *2*(4), 1152–1167.

Kopfstedt, T., Mukai, M., Fujita, M., & Ament, C. (2008). Control of formations of UAVs for surveillance and reconnaissance missions , In *Proceedings of 17th IFAC World Congress*, Seoul, South Korea: IFAC (pp. 6–11).

Krick, L., Broucke, M.E., & Francis, B.A. (2009). Stabilisation of infinitesimally rigid formations of multi-robot networks. *International Journal of Control*, *82*(3), 423–439.

Krieger, G., Hajnsek, I., Papathanassiou, K.P., Younis, M., & Moreira, A. (2010). Interferometric synthetic aperture radar (SAR) missions employing formation flying. *Proceedings of the IEEE*, *98*(5), 816–843.

Krstic, M., & Smyshlyaev, A. (2008). *Boundary control of PDEs: A course on backstepping designs*. Philadelphia, PA: SIAM.
LeVeque, R.J. (2007). *Finite difference methods for ordinary and partial differential equations: Steady-state and time-dependent problems*. Philadelphia, PA: SIAM.
Mauroy, A., & Sepulchre, R. (2013). Global analysis of a continuum model for monotone pulse-coupled oscillators. *IEEE Transactions on Automatic Control*, *58*(5), 1154–1166.
Meurer, T. (2013). *Control of higher-dimensional PDEs*. Berlin: Springer.
Meurer, T., & Krstic, M. (2011). Finite-time multi-agent deployment: A nonlinear PDE motion planning approach. *Automatica*, *47*(11), 2534–2542.
Oh, K.K., Park, M.C., & Ahn, H.S. (2015). A survey of multi-agent formation control. *Automatica*, *53*, 424–440.
Olfati-Saber, R., Fax, J., & Murray, R. (2007). Consensus and cooperation in networked multi-agent systems. *Proceedings of the IEEE*, *95*(1), 215–233.
Olfati-Saber, R., & Murray, R.M. (2004). Consensus problems in networks of agents with switching topology and time-delays. *IEEE Transactions on Automatic Control*, *49*(9), 1520–1533.
Qi, J. (2016). Simulation movie of an example 3-D formation control. Retrieved from https://www.dropbox.com/s/5xmkiepgygjgqtw/transobs.mp4?dl=0
Qi, J., Vázquez, R., & Krstic, M. (2015). Multi-agent deployment in 3-D via PDE control. *IEEE Transactions on Automatic Control*, *60*(4), 891–906.
Ren, W., Beard, R.W., & Atkins, E.M. (2005). A survey of consensus problems in multi-agent coordination. In *IEEE American control conference*, Portland: IEEE (pp. 1859–1864).
Ren, W., & Sorensen, N. (2008). Distributed coordination architecture for multi-robot formation control. *Robotics and Autonomous Systems*, *56*(4), 324–333.
Sarlette, A., & Sepulchre, R. (2009). A PDE viewpoint on basic properties of coordination algorithms with symmetries. In *48th IEEE conference on decision and control and 28th IEEE Chinese control conference*, Shanghai, China: IEEE (pp. 5139–5144).
Shiroma, N., Chiu, Y.H., Sato, N., & Matsuno, F. (2005). Cooperative task execution of a search and rescue mission by a multi-robot team. *Advanced Robotics*, *19*(3), 311–329.
Smyshlyaev, A., & Krstic, M. (2004). Closed-form boundary state feedbacks for a class of 1-D partial integro-differential equations. *IEEE Transactions on Automatic Control*, *49*(12), 2185–2202.
Tavakoli, M., Cabrita, G., Faria, R., Marques, L., & de Almeida, A.T. (2012). Cooperative multi-agent mapping of three-dimensional structures for pipeline inspection applications. *The International Journal of Robotics Research*, *31*(12), 1489–1503.
Vázquez, R., & Krstic, M. (2007). A closed-form feedback controller for stabilization of the linearized 2-D Navier–Stokes Poiseuille system. *IEEE Transactions on Automatic Control*, *52*(12), 2298–2312.
Vázquez, R., Trélat, E., & Coron, J.M. (2008). Control for fast and stable laminar-to-high-Reynolds-numbers transfer in a 2D Navier–Stokes channel flow. *Discrete and Continuous Dynamical Systems-Series B*, *10*(4), 925–956.
Wang, X., & Su, H. (2014). Pinning control of complex networked systems: A decade after and beyond. *Annual Reviews in Control*, *38*(1), 103–111.
Xu, C., Dong, Y., Ren, Z., Jiang, H., & Yu, X. (2014). Sensor deployment for pipeline leakage detection via optimal boundary control strategies. *Journal of Industrial and Management Optimization*, *11*(1), 199–216.
Zhang, F., & Leonard, N. (2010). Cooperative filters and control for cooperative exploration. *IEEE Transactions on Automatic Control*, *55*(3), 650–663.

Appendices

Appendix 1. Equivalence between a complex-valued reaction–advection–diffusion PDE and the corresponding PDE with zero-advection term

Consider the following complex-valued PDE:

$$u_t(t,\theta,s) = u_{\theta\theta}(t,\theta,s) + u_{ss}(t,\theta,s) + \beta_1 u_s(t,\theta,s) + \lambda_1 u(t,\theta,s), \quad \text{(A1)}$$

$$u(t,\theta,0) = 0, \quad \text{(A2)}$$

$$u(t,\theta,1) = U(t,\theta), \quad \text{(A3)}$$

$$u(t,0,s) = u(t,2\pi,s). \quad \text{(A4)}$$

Define the real and imaginary parts of u, U, β_1 and λ_1, respectively, as

$$\breve{\rho} = \mathrm{Re}(u), \quad \breve{\iota} = \mathrm{Im}(u), \quad \text{(A5)}$$

$$U_R = \mathrm{Re}(U), \quad U_I = \mathrm{Im}(U), \quad \text{(A6)}$$

$$\beta_R = \mathrm{Re}(\beta_1), \quad \beta_I = \mathrm{Im}(\beta_1), \quad \text{(A7)}$$

$$\lambda_R = \mathrm{Re}(\lambda_1), \quad \lambda_I = \mathrm{Im}(\lambda_1). \quad \text{(A8)}$$

Then, Equations (A1)–(A4) become

$$\breve{\rho}_t = \breve{\rho}_{\theta\theta} + \breve{\rho}_{ss} + \beta_R\breve{\rho}_s - \beta_I\breve{\iota}_s + \lambda_R\breve{\rho} - \lambda_I\breve{\iota}, \quad \text{(A9)}$$

$$\breve{\iota}_t = \breve{\iota}_{\theta\theta} + \breve{\iota}_{ss} + \beta_R\breve{\iota}_s + \beta_I\breve{\rho}_s + \lambda_R\breve{\iota} + \lambda_I\breve{\rho}, \quad \text{(A10)}$$

for $(t,\theta,s) \in \mathbb{R}^+ \times \Omega$, with the boundary conditions

$$\breve{\rho}(t,\theta,0) = 0, \quad \breve{\rho}(t,\theta,1) = \tilde{U}_R(t,\theta), \quad \text{(A11)}$$

$$\breve{\rho}(t,0,s) = \breve{\rho}(t,2\pi,s), \quad \text{(A12)}$$

$$\breve{\iota}(t,\theta,0) = 0, \quad \breve{\iota}(t,\theta,1) = \tilde{U}_I(t,\theta), \quad \text{(A13)}$$

$$\breve{\iota}(t,0,s) = \breve{\iota}(t,2\pi,s). \quad \text{(A14)}$$

Introducing the transformation

$$\rho = \mathrm{e}^{\frac{1}{2}\beta_R s}\left(\breve{\rho}\cos\left(\frac{1}{2}\beta_I s\right) - \breve{\iota}\sin\left(\frac{1}{2}\beta_I s\right)\right), \quad \text{(A15)}$$

$$\iota = \mathrm{e}^{\frac{1}{2}\beta_R s}\left(\breve{\rho}\sin\left(\frac{1}{2}\beta_I s\right) + \breve{\iota}\cos\left(\frac{1}{2}\beta_I s\right)\right), \quad \text{(A16)}$$

then, one can show that the new states ρ and ι satisfy

$$\rho_t = \rho_{\theta\theta} + \rho_{ss} + \bar{\lambda}_R\rho - \bar{\lambda}_I\iota, \quad \text{(A17)}$$

$$\iota_t = \iota_{\theta\theta} + \iota_{ss} + \bar{\lambda}_I\rho + \bar{\lambda}_R\iota, \quad \text{(A18)}$$

where

$$\bar{\lambda}_R = \lambda_R - \frac{1}{4}\left(\beta_R^2 - \beta_I^2\right), \bar{\lambda}_I = \lambda_I - \frac{1}{2}\beta_R\beta_I, \quad \text{(A19)}$$

which is consistent with (33), and the boundary conditions are

$$\rho(t,\theta,0) = 0, \quad \rho(t,\theta,1) = V_R(t,\theta), \quad \text{(A20)}$$

$$\rho(t,0,s) = \rho(t,2\pi,s), \quad \text{(A21)}$$

$$\iota(t,\theta,0) = 0, \quad \iota(t,\theta,1) = V_I(t,\theta), \quad \text{(A22)}$$

$$\iota(t,0,s) = \iota(t,2\pi,s). \quad \text{(A23)}$$

Let

$$\upsilon = \rho + \mathrm{j}\iota, \quad \text{(A24)}$$

then, we can get from (A17) to (A18) the following complex-valued equation:

$$\upsilon_t = \upsilon_{\theta\theta} + \upsilon_{ss} + \lambda\upsilon, \quad \text{(A25)}$$

where

$$\lambda = \lambda_1 - \frac{1}{4}\beta_1^2 = \lambda_R - \frac{1}{4}\left(\beta_R^2 - \beta_I^2\right) + \mathrm{j}\left(\lambda_I - \frac{1}{2}\beta_R\beta_I\right), \quad \text{(A26)}$$

with the boundary conditions

$$\upsilon(t,\theta,0) = 0, \quad \upsilon(t,\theta,1) = V(t,\theta), \quad \text{(A27)}$$

$$\upsilon(t,0,s) = \upsilon(t,2\pi,s), \quad \text{(A28)}$$

where

$$V = V_R + \mathrm{j}V_I. \quad \text{(A29)}$$

Note that the transformation between u and υ is invertible. Indeed, we have from (A5), (A15), (A16) and (A24) the following direct and inverse transformations between u and υ:

$$\upsilon = \mathrm{e}^{\frac{1}{2}\beta_R s}\left(\mathrm{Re}(u)\cos\left(\frac{1}{2}\beta_I s\right) - \mathrm{Im}(u)\sin\left(\frac{1}{2}\beta_I s\right)\right) + \mathrm{j}\mathrm{e}^{\frac{1}{2}\beta_R s}\left(\mathrm{Re}(u)\sin\left(\frac{1}{2}\beta_I s\right) + \mathrm{Im}(u)\cos\left(\frac{1}{2}\beta_I s\right)\right), \quad \text{(A30)}$$

$$u = \mathrm{e}^{-\frac{1}{2}\beta_R s}\left(\mathrm{Re}(\upsilon)\cos\left(\frac{1}{2}\beta_I s\right) + \mathrm{Im}(\upsilon)\sin\left(\frac{1}{2}\beta_I s\right)\right) + \mathrm{j}\mathrm{e}^{-\frac{1}{2}\beta_R s}\left(\mathrm{Im}(\upsilon)\cos\left(\frac{1}{2}\beta_I s\right) - \mathrm{Re}(\upsilon)\sin\left(\frac{1}{2}\beta_I s\right)\right). \quad \text{(A31)}$$

Thus, Equations (A1)–(A4) and the Equations (A25), (A27) and (A28) are equivalent.

Appendix 2. Equivalence between the control designs for the complex-valued PDE (30)–(32) and for the corresponding coupled real-valued PDE systems

In this section, we will show that the control design for the complex-valued PDE (30)–(32) is equivalent to that for the two coupled real-valued PDEs corresponding to the real part and imaginary parts of (30)–(32), respectively. The Fourier series expansion of the real-valued states ρ and ι are

$$\rho(t,\theta,s) = \frac{1}{2}a_0(t,s) + \sum_{n=1}^{\infty}\left(a_n(t,s)\cos(n\theta) + b_n(t,s)\sin(n\theta)\right), \quad \text{(B1)}$$

$$\iota(t,\theta,s) = \frac{1}{2}c_0(t,s) + \sum_{n=1}^{\infty}\left(c_n(t,s)\cos(n\theta) + d_n(t,s)\sin(n\theta)\right), \quad \text{(B2)}$$

where the coefficients are

$$a_n(t,s) = \frac{1}{\pi}\int_{-\pi}^{\pi}\rho(t,\theta,s)\cos(n\theta)d\theta,$$
$$b_n(t,s) = \frac{1}{\pi}\int_{-\pi}^{\pi}\rho(t,\theta,s)\sin(n\theta)d\theta, \quad \text{(B3)}$$
$$c_n(t,s) = \frac{1}{\pi}\int_{-\pi}^{\pi}\iota(t,\theta,s)\cos(n\theta)d\theta,$$
$$d_n(t,s) = \frac{1}{\pi}\int_{-\pi}^{\pi}\iota(t,\theta,s)\sin(n\theta)d\theta. \quad \text{(B4)}$$

Note that the Fourier series expansion reduces the angular dependence of the state. Substituting (B1) and (B2) into the coupled PDEs (A17)–(A23), we get two groups

of PDEs as follows:

$$a_{nt}(t,s) = a_{nss}(t,s) - n^2 a_n(t,s) + \bar{\lambda}_R a_n(t,s) - \bar{\lambda}_I c_n(t,s), \tag{B5}$$

$$c_{nt}(t,s) = c_{nss}(t,s) - n^2 c_n(t,s) + \bar{\lambda}_R c_n(t,s) + \bar{\lambda}_I a_n(t,s), \tag{B6}$$

$$a_n(t,0) = 0, \quad c_n(t,0) = 0, \quad a_n(t,1) = V_{n1}(t), \quad c_n(t,1) = V_{n3}(t), \tag{B7}$$

$$b_{nt}(t,s) = b_{nss}(t,s) - n^2 b_n(t,s) + \bar{\lambda}_R b_n(t,s) - \bar{\lambda}_I d_n(t,s), \tag{B8}$$

$$d_{nt}(t,s) = d_{nss}(t,s) - n^2 d_n(t,s) + \bar{\lambda}_R d_n(t,s) + \bar{\lambda}_I b_n(t,s), \tag{B9}$$

$$b_n(t,0) = 0, \quad d_n(t,0) = 0, \quad b_n(t,1) = V_{n2}(t), \quad d_n(t,1) = V_{n4}(t), \tag{B10}$$

where V_{n1}, V_{n2}, V_{n3}, V_{n4} are boundary controllers to be designed. (B5)–(B7) is a coupled system of unstable PDEs, which can be transformed to the following stable target system

$$\breve{a}_{nt}(t,s) = \breve{a}_{nss}(t,s) - n^2 \breve{a}_n(t,s), \tag{B11}$$

$$\breve{c}_{nt}(t,s) = \breve{c}_{nss}(t,s) - n^2 \breve{c}_n(t,s), \tag{B12}$$

$$\breve{a}_n(t,0) = 0, \quad \breve{c}_n(t,0) = 0, \quad \breve{a}_n(t,1) = 0, \quad \breve{c}_n(t,1) = 0 \tag{B13}$$

by the transformation

$$\breve{a}_n(t,s) = a_n(t,s) - \int_0^s k_n(s,\tau) a_n(t,\tau) d\tau + \int_0^s k_{In}(s,\tau) c_n(t,\tau) d\tau, \tag{B14}$$

$$\breve{c}_n(t,s) = c_n(t,s) - \int_0^s k_{In}(s,\tau) a_n(t,\tau) d\tau - \int_0^s k_n(s,\tau) c_n(t,\tau) d\tau. \tag{B15}$$

By calculation, we can get the following kernel equations:

$$k_{nss}(s,\tau) - k_{n\tau\tau}(s,\tau) - \bar{\lambda}_R k_n(s,\tau) + \bar{\lambda}_I k_{In}(s,\tau) = 0, \tag{B16}$$

$$k_{Inss}(s,\tau) - k_{In\tau\tau}(s,\tau) - \bar{\lambda}_R k_{In}(s,\tau) - \bar{\lambda}_I k_n(s,\tau) = 0, \tag{B17}$$

$$k_n(s,0) = 0, \quad k_n(s,s) = -\frac{1}{2}\bar{\lambda}_R s, \tag{B18}$$

$$k_{In}(s,0) = 0, \quad k_{In}(s,s) = -\frac{1}{2}\bar{\lambda}_I s. \tag{B19}$$

Introducing the change of variables

$$\zeta = s + \tau, \quad \eta = s - \tau \tag{B20}$$

and new functions $q_R(\zeta,\eta) = k_n(s,\tau)$, $q_I(\zeta,\eta) = k_{In}(s,\tau)$, we have the transformed kernel equations

$$q_{R\zeta\eta}(\zeta,\eta) = \frac{\bar{\lambda}_R}{4} q_R - \frac{\bar{\lambda}_I}{4} q_I, \tag{B21}$$

$$q_{I\zeta\eta}(\zeta,\eta) = \frac{\bar{\lambda}_I}{4} q_R + \frac{\bar{\lambda}_R}{4} q_I, \tag{B22}$$

$$q_R(\zeta,\zeta) = 0, \quad q_R(\zeta,0) = -\frac{\bar{\lambda}_R}{4}\zeta, \tag{B23}$$

$$q_I(\zeta,\zeta) = 0, \quad q_I(\zeta,0) = -\frac{\bar{\lambda}_I}{4}\zeta. \tag{B24}$$

Integrating (B21) and (B22) twice, we get

$$q_R(\zeta,\eta) = q_R(\zeta,0) - q_R(\eta,0) + \int_\eta^\zeta \int_0^\eta \left(\frac{\bar{\lambda}_R}{4} q_R(\gamma,\mu) - \frac{\bar{\lambda}_I}{4} q_I(\gamma,\mu) \right) d\mu d\gamma, \tag{B25}$$

$$q_I(\zeta,\eta) = q_I(\zeta,0) - q_I(\eta,0) + \int_\eta^\zeta \int_0^\eta \left(\frac{\bar{\lambda}_I}{4} q_R(\gamma,\mu) + \frac{\bar{\lambda}_R}{4} q_I(\gamma,\mu) \right) d\mu d\gamma. \tag{B26}$$

We use next a classical iterative method in order to prove that the coupled Equations (B25) and (B26) have a unique solution. Let us start with initial functions $q_R^0(\zeta,\eta) = 0$ and $q_I^0(\zeta,\eta) = 0$, and set up the following recursion for $l = 0, 1, 2, \ldots$:

$$q_R^{l+1}(\zeta,\eta) = -\frac{\bar{\lambda}_R}{4}(\zeta - \eta) + \int_\eta^\zeta \int_0^\eta \left(\frac{\bar{\lambda}_R}{4} q_R^l(\gamma,\mu) - \frac{\bar{\lambda}_I}{4} q_I^l(\gamma,\mu) \right) d\mu d\gamma, \tag{B27}$$

$$q_I^{l+1}(\zeta,\eta) = -\frac{\bar{\lambda}_I}{4}(\zeta - \eta) + \int_\eta^\zeta \int_0^\eta \left(\frac{\bar{\lambda}_I}{4} q_R^l(\gamma,\mu) + \frac{\bar{\lambda}_R}{4} q_I^l(\gamma,\mu) \right) d\mu d\gamma. \tag{B28}$$

Denote the difference between two consecutive terms by

$$\begin{aligned}\Delta q_R^l(\zeta,\eta) &= q_R^{l+1}(\zeta,\eta) - q_R^l(\zeta,\eta)\\ &= \int_\eta^\zeta \int_0^\eta \left(\frac{\bar{\lambda}_R}{4}\Delta q_R^{l-1}(\gamma,\mu)\right.\\ &\quad \left. - \frac{\bar{\lambda}_I}{4}\Delta q_I^{l-1}(\gamma,\mu)\right) d\mu d\gamma, \quad \text{(B29)}\\ \Delta q_I^l(\zeta,\eta) &= q_I^{l+1}(\zeta,\eta) - q_I^l(\zeta,\eta)\\ &= \int_\eta^\zeta \int_0^\eta \left(\frac{\bar{\lambda}_I}{4}\Delta q_R^{l-1}(\gamma,\mu)\right.\\ &\quad \left. + \frac{\bar{\lambda}_R}{4}\Delta q_I^{l-1}(\gamma,\mu)\right) d\mu d\gamma, \quad \text{(B30)}\end{aligned}$$

then,

$$q_R(\zeta,\eta) = \sum_{l=0}^{\infty} \Delta q_R^l, \quad q_I(\zeta,\eta) = \sum_{l=0}^{\infty} \Delta q_I^l. \quad \text{(B31)}$$

Starting with $\Delta q_R^0(\zeta,\eta) = -\frac{\bar{\lambda}_R}{4}(\zeta-\eta)$ and $\Delta q_I^0(\zeta,\eta) = -\frac{\bar{\lambda}_I}{4}(\zeta-\eta)$, we derive by induction that

$$\begin{aligned}\Delta q_R^l(\zeta,\eta) &= -\left(\frac{1}{4}\right)^{l+1} \sum_{m=0}^{\lfloor\frac{l+1}{2}\rfloor}\\ &\quad \times \left((-1)^m \frac{(l+1)!}{2m!(l+1-2m)!}\bar{\lambda}_R^{l+1-2m}\bar{\lambda}_I^{2m}\right)\\ &\quad \times \frac{\zeta^l\eta^l}{l!(l+1)!}(\zeta-\eta), \quad \text{(B32)}\\ \Delta q_I^l(\zeta,\eta) &= -\left(\frac{1}{4}\right)^{l+1} \sum_{m=0}^{\lfloor\frac{l}{2}\rfloor}\\ &\quad \times \left((-1)^m \frac{(l+1)!}{(2m+1)!(l-2m)!}\bar{\lambda}_R^{l-2m}\bar{\lambda}_I^{2m+1}\right)\\ &\quad \times \frac{\zeta^l\eta^l}{l!(l+1)!}(\zeta-\eta). \quad \text{(B33)}\end{aligned}$$

Note that the above equations can be rewritten as

$$\begin{aligned}&\Delta q_R^{l+1}(\zeta,\eta)\\ &= -\left(\frac{1}{4}\right)^{l+1} \mathrm{Re}\left((\bar{\lambda}_R + \mathrm{j}\bar{\lambda}_I)^{l+1}\right) \frac{\zeta^l\eta^l}{l!(l+1)!}(\zeta-\eta), \quad \text{(B34)}\\ &\Delta q_I^{l+1}(\zeta,\eta)\\ &= -\left(\frac{1}{4}\right)^{l+1} \mathrm{Im}\left((\bar{\lambda}_R + \mathrm{j}\bar{\lambda}_I)^{l+1}\right) \frac{\zeta^l\eta^l}{l!(l+1)!}(\zeta-\eta), \quad \text{(B35)}\end{aligned}$$

then the solutions of (B25) and (B26) are

$$\begin{aligned}q_R(\zeta,\eta) &= -\sum_{l=0}^{\infty}\left(\frac{1}{4}\right)^{l+1} \mathrm{Re}\left((\bar{\lambda}_R + \mathrm{j}\bar{\lambda}_I)^{l+1}\right)\\ &\quad \times \frac{\zeta^l\eta^l}{l!(l+1)!}(\zeta-\eta), \quad \text{(B36)}\\ q_I(\zeta,\eta) &= -\sum_{l=0}^{\infty}\left(\frac{1}{4}\right)^{l+1} \mathrm{Im}\left((\bar{\lambda}_R + \mathrm{j}\bar{\lambda}_I)^{l+1}\right)\\ &\quad \times \frac{\zeta^l\eta^l}{l!(l+1)!}(\zeta-\eta). \quad \text{(B37)}\end{aligned}$$

Recalling the fist-order modified Bessel function in form of series, we have

$$q_R(\zeta,\eta) = -\mathrm{Re}\left((\bar{\lambda}_R + \mathrm{j}\bar{\lambda}_I)(\zeta-\eta)\frac{\mathrm{I}_1\sqrt{(\bar{\lambda}_R + \mathrm{j}\bar{\lambda}_I)\zeta\eta}}{2\sqrt{(\bar{\lambda}_R + \mathrm{j}\bar{\lambda}_I)\zeta\eta}}\right), \quad \text{(B38)}$$

$$q_I(\zeta,\eta) = -\mathrm{Im}\left((\bar{\lambda}_R + \mathrm{j}\bar{\lambda}_I)(\zeta-\eta)\frac{\mathrm{I}_1\sqrt{(\bar{\lambda}_R + \mathrm{j}\bar{\lambda}_I)\zeta\eta}}{2\sqrt{(\bar{\lambda}_R + \mathrm{j}\bar{\lambda}_I)\zeta\eta}}\right). \quad \text{(B39)}$$

Returning to the original s, τ variables, the following kernel functions are obtained:

$$k_n(s,\tau) = -\mathrm{Re}\left((\bar{\lambda}_R + \mathrm{j}\bar{\lambda}_I)\tau\frac{\mathrm{I}_1\sqrt{(\bar{\lambda}_R + \mathrm{j}\bar{\lambda}_I)(s^2-\tau^2)}}{\sqrt{(\bar{\lambda}_R + \mathrm{j}\bar{\lambda}_I)(s^2-\tau^2)}}\right), \quad \text{(B40)}$$

$$k_{In}(s,\tau) = -\mathrm{Im}\left((\bar{\lambda}_R + \mathrm{j}\bar{\lambda}_I)\tau\frac{\mathrm{I}_1\sqrt{(\bar{\lambda}_R + \mathrm{j}\bar{\lambda}_I)(s^2-\tau^2)}}{\sqrt{(\bar{\lambda}_R + \mathrm{j}\bar{\lambda}_I)(s^2-\tau^2)}}\right). \quad \text{(B41)}$$

Hence, the real part of (46) is (B40), and the imaginary part of (46) is (B41):

$$k_n(s,\tau) = \mathrm{Re}(K(s,\tau)), \quad k_{In}(s,\tau) = \mathrm{Im}(K(s,\tau)). \quad \text{(B42)}$$

Similar to the complex-valued kernel, all the kernels $k_n(s,\tau)$ and $k_{In}(s,\tau)$ are independent of n, and, thus, we write

$$k_n(s,\tau) \triangleq k(s,\tau), \quad k_{In}(s,\tau) \triangleq k_I(s,\tau). \quad \text{(B43)}$$

Combined (B13), (B14) and (B15), the controllers for a_n, c_n are

$$a_n(t,1)=\int_0^1 (k(1,\tau)a_n(t,\tau)-k_I(1,\tau)c_n(t,\tau))d\tau, \tag{B44}$$

$$c_n(t,1)=\int_0^1 (k_I(1,\tau)a_n(t,\tau)+k(1,\tau)c_n(t,\tau))d\tau. \tag{B45}$$

(B8)–(B10) has the same form as (B5)–(B7) and can be dealt with in the same way as above. Indeed, for the coupled unstable Equations (B8)–(B10), we introduce a similar transformation

$$\breve{b}_n=b_n-\int_0^s k_{2n}(s,\tau)b_n(\tau)d\tau-\int_0^s k_{2nI}(s,\tau)d_n(\tau)d\tau, \tag{B46}$$

$$\breve{d}_n=d_n+\int_0^s k_{2nI}(s,\tau)b_n(\tau)d\tau-\int_0^s k_{2n}(s,\tau)d_n(\tau)d\tau, \tag{B47}$$

and get the target system as follows:

$$\breve{b}_{nt}(t,s)=\breve{b}_{nss}(t,s)-n^2\breve{b}_n(t,s), \tag{B48}$$

$$\breve{d}_{nt}(t,s)=\breve{d}_{nss}(t,s)-n^2\breve{d}_n(t,s), \tag{B49}$$

$$\breve{b}_n(t,0)=0,\quad \breve{b}_n(t,0)=0,\quad \breve{d}_n(t,1)=0,\quad \breve{d}_n(t,1)=0. \tag{B50}$$

The kernel functions for (B8)–(B10) are the same as (B40) and (B41):

$$k_{2n}(s,\tau)=k_n(s,\tau),\quad k_{2nI}(s,\tau)=k_{In}(s,\tau), \tag{B51}$$

and the controllers are

$$b_n(t,1)=\int_0^1 (k(1,\tau)b_n(t,\tau)-k_I(1,\tau)d_n(t,\tau))d\tau, \tag{B52}$$

$$d_n(t,1)=\int_0^1 (k_I(1,\tau)b_n(t,\tau)+k(1,\tau)d_n(t,\tau))d\tau. \tag{B53}$$

Recalling (B1) and (B2), we have the real part of the boundary controller as

$$\begin{aligned}V_R(t,\theta)=\rho(t,\theta,1)&=\frac{1}{2}a_0(t,1)+\sum_{n=1}^{\infty}(a_n(t,1)\cos(n\theta)\\&\quad+b_n(t,1)\sin(n\theta))\\&=\int_0^1 k(1,\tau)\Big[\frac{1}{2}a_0(t,\tau)+\sum_{n=1}^{\infty}(a_n(t,\tau)\cos(n\theta)\\&\quad+b_n(t,\tau)\sin(n\theta))\Big]d\tau-\int_0^1 k_I(1,\tau)\\&\quad\times\Big[\frac{1}{2}c_0(t,\tau)+\sum_{n=1}^{\infty}(c_n(t,\tau)\cos(n\theta)\\&\quad+d_n(t,\tau)\sin(n\theta))\Big]d\tau\\&=\int_0^1 (k(1,\tau)\rho(t,\theta,\tau)\\&\quad-k_I(t,\tau)\iota(t,\theta,\tau))d\tau.\end{aligned} \tag{B54}$$

In the same way, we have the imaginary part as

$$\begin{aligned}V_I(t,\theta)=\iota(t,\theta,1)=\int_0^1 (k_I(1,\tau)\rho(t,\theta,\tau)\\-k(t,\tau)\iota(t,\theta,\tau))d\tau.\end{aligned} \tag{B55}$$

From (B42), we conclude that (B54) and (B55) are exactly the real part and imaginary part of the controller in complex-valued form (53). Therefore, the equivalence between the control designs for the complex-valued PDE and for the corresponding coupled real-valued PDE systems is proved.